iScience

CellPress
OPEN ACCESS

Article

Design, synthesis and mechanistic anticancer activity of new acetylated 5-aminosalicylate-thiazolinone hybrid derivatives

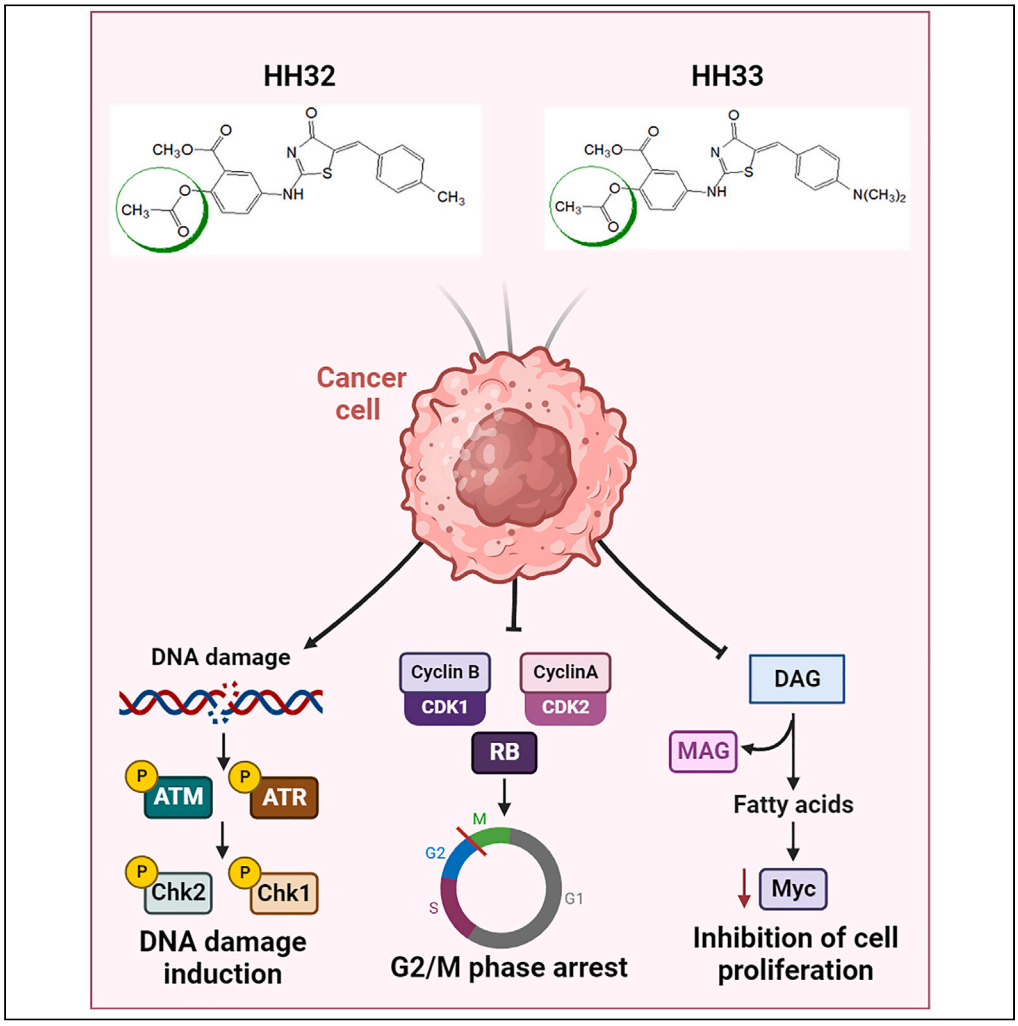

Wafaa S. Ramadan, Maha M. Saber-Ayad, Ekram Saleh, ..., Osamu Kanie, Rifat Hamoudi, Raafat El-Awady

relawady@sharjah.ac.ae

Highlights

Development of acetylated hybrids with antiproliferative activity on cancer cells

Structural data indicate the binding of the hybrid compounds to cell cycle regulators

Hybrid compounds induce DNA damage and arrest cancer cells at the G2/M phase

Hybrid compounds modulate the metabolomic profile of cancer cells

Ramadan et al., iScience 27, 108659
January 19, 2024
https://doi.org/10.1016/j.isci.2023.108659

iScience

CellPress
OPEN ACCESS

Article

Design, synthesis and mechanistic anticancer activity of new acetylated 5-aminosalicylate-thiazolinone hybrid derivatives

Wafaa S. Ramadan,[1,9] Maha M. Saber-Ayad,[1,3,9] Ekram Saleh,[4] Hajjaj H.M. Abdu-Allah,[5] Abdel-nasser A. El-Shorbagi,[2,5] Varsha Menon,[1] Hamadeh Tarazi,[2] Mohammad H. Semreen,[2] Nelson C. Soares,[1,2] Shirin Hafezi,[1] Thenmozhi Venkatakhalam,[1] Samrein Ahmed,[1,8] Osamu Kanie,[6] Rifat Hamoudi,[1,3,7] and Raafat El-Awady[1,2,10,*]

SUMMARY

The development of hybrid compounds has been widely considered as a promising strategy to circumvent the difficulties that emerge in cancer treatment. The well-established strategy of adding acetyl groups to certain drugs has been demonstrated to enhance their therapeutic efficacy. Based on our previous work, an approach of accommodating two chemical entities into a single structure was implemented to synthesize new acetylated hybrids (HH32 and HH33) from 5-aminosalicylic acid and 4-thiazolinone derivatives. These acetylated hybrids showed potential anticancer activities and distinct metabolomic profile with antiproliferative properties. The *in-silico* molecular docking predicts a strong binding of HH32 and HH33 to cell cycle regulators, and transcriptomic analysis revealed DNA repair and cell cycle as the main targets of HH33 compounds. These findings were validated using *in vitro* models. In conclusion, the pleiotropic biological effects of HH32 and HH33 compounds on cancer cells demonstrated a new avenue to develop more potent cancer therapies.

INTRODUCTION

The development of anticancer hybrid compounds has drawn interest as a potential strategy in drug discovery to tackle the present challenges in cancer therapy. This approach involved the molecular hybridization of two drug pharmacophores into a single molecule with a distinct mode of action on several targets. Drugs with multicellular targets might partially replace the use of combination chemotherapy and thus decrease the risk of development of resistance.[1] Consequently, many efforts have been made to design several hybrid compounds with anticancer activities. Interestingly, various hybrid compounds containing 1,2,3-Triazole, which is an important pharmacophore used in the molecular hybridization approach, have been evaluated as lead compounds for diverse biological targets. Indeed, the 1,2,3-Triazole-containing hybrids have been widely demonstrated to have antioxidant and anticancer activities.[2–4]

Although salicylic acid was first prepared in 1838, it is still an attractive compound that inspires chemists to synthesize new derivatives for the treatment of several diseases.[5] Thiazolinones, on the other hand, are recognized to induce a myriad of anticancer effects.[6–11] We have previously developed a group of compounds with promising anti-cancer activity by combining 5-aminosalicylic acid (5-ASA) with 4-thiazolinone.[12] Screening and testing the activity of such compounds on cancer and normal cells identified four compounds with good anti-cancer activity and some degree of selectivity toward cancer cells.[13]

The main structural differences between these two new derivatives (**HH32** and **HH33**) and the formerly developed ones (**HH3** and **HH13**) are the acetylation of the phenolic OH of the 5-ASA in the new compounds (Figure 1). Intriguingly, acetylation of salicylic acid to produce acetyl salicylic acid (Aspirin) has long been shown to improve the therapeutic potential of the former.[14] Aspirin exhibits pharmacokinetics and pharmacodynamics superior to salicylic acid.[15] The *O*-acetyl group in aspirin has long been recognized as an important contributor to its diverse effects.[16] *in vitro* and *in vivo* evidences demonstrated that aspirin, but not salicylic acid, acetylates macromolecules such as

[1]Research Institute for Medical and Health Sciences, University of Sharjah, Sharjah 27272, United Arab Emirates
[2]College of Pharmacy, University of Sharjah, Sharjah 27272, United Arab Emirates
[3]College of Medicine, University of Sharjah, Sharjah 27272, United Arab Emirates
[4]Medical Biochemistry and Molecular Biology Unit, Cancer Biology Department, National Cancer Institute, Cairo University, Cairo 12613, Egypt
[5]Faculty of Pharmacy, Assiut University, Assiut 16122, Egypt
[6]Department of Applied Biochemistry, Tokai University, 4-1-1 Kitakaname, Hiratsuka, Kanagawa 259-1292, Japan
[7]Division of Surgery and Interventional Science, Faculty of Medical Science, University College London, London, United Kingdom
[8]Department of Biosciences and Chemistry, College of Health, Wellbeing and Life sciences, University of Sheffield Hallam, Sheffield S1 1WB, United Kingdom
[9]These authors contributed equally
[10]Lead contact
*Correspondence: relawady@sharjah.ac.ae
https://doi.org/10.1016/j.isci.2023.108659

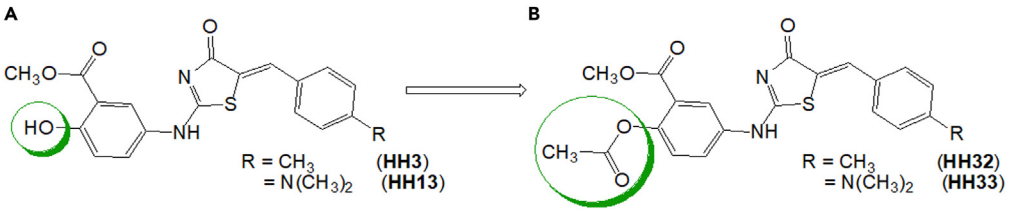

Figure 1. Chemical structure of HH compounds

(A) Structure of non-acetylated compounds (**HH3** and **HH13**).

(B) Structure of acetylated compounds (**HH32** and **HH33**).

hemoglobin, serum albumin, various proteins (enzymes and hormones) and membrane of platelet and of red blood cells.[17] On the cellular level, aspirin can acetylate several proteins and biomolecules, such as DNA, RNA, histones, and transglutaminase.[18,19]

Recently, it has been shown that aspirin, at micromolar concentration, acetylates the tumor suppressor protein p53, a known regulator of apoptosis, in different types of cancer. This effect was associated with the induction of $p21^{Cip1}$, a protein involved in cell-cycle arrest, and Bax, a proapoptotic protein.[20,21] Furthermore, aspirin directly interacts with p300 acetyltransferase in the nucleus to promote the acetylation of histone 3 at lysine 9 (H3K9), which activates Fas ligand expression and induces apoptosis in colorectal cancer stem cells (CSCs).[22] Acetylation of glucose-6-phosphate dehydrogenase (G6PD) at several sites could inhibit G6PD activity, which may contribute to the ability of aspirin to exert anticancer effects through decreased synthesis of ribose sugars and NADPH.[23] These acetylation events are thought to be the mediators of aspirin's anti-cancer activity. Interestingly, another evidence that the acetylation of compounds enhances their pharmacological activity is deduced from the narcotic analgesic heroin – a di-acetylated derivative of morphine-which is more active than morphine.[24] Also, the acetylated resveratrol analogues demonstrate an improved anticancer potencies.[25] All of these evidences about the valuable contribution of the acetyl group to the biological activities together with the promising biological results of HH series, inspired us to do QSAR studies. The results from these studies encouraged us to synthesize the acetylated derivatives (**HH32** and **HH33**) of the two most active compounds (**HH3** and **HH13**) from our previous studies. This inspired us to check the anticancer effects of acetylating our previously developed 5-ASA-4-thiazolinone compounds[13] and to reveal their anticancer mechanisms.

To optimize the compounds' potency and selectivity, the QSAR study was carried out. A QSAR study of 45 compounds[12,13,26,27] against the MCF7 cancer cell line under the same conditions was done. A multiple linear regression equation of eight parameters represents the best developed model capable of describing the inhibitory pattern against MCF7 cells (Figure 2). Calculations using this model suggested two candidate compounds (**HH32** and **HH33**) providing up to 100% growth inhibition. These candidate compounds were then synthesized (Scheme 1 and Figure 3) and subjected to pharmacological investigation.

The aim of the present study is to synthesize pre-determined highly potent and selective acetylsalicylate-4-thiazolinone hybrid derivatives developed depending on *in silico* detection. Also, to investigate their anti-proliferative effects, selectivity, and potential mechanisms of anticancer activity.

RESULTS

Acetylated 5-aminosalicylate-thiazolinone hybrid derivatives exhibited cytotoxicity toward cancer cells.

Both **HH32** and **HH33** compounds induced a remarkable concentration-dependent decrease in the viability of the eight tested cancer cell lines (Figures S1A—S1H and Table 1). The results in Table 1 show that **HH33** derivative exhibited higher anti-proliferative effects than **HH32**. In particular, four cell lines (MCF7, HeLa, HCT-116, and HepG2) were highly sensitive to the **HH33** with IC_{50} values less than 1 μM, whereas the other four cell lines (A549, MDA-MB-231, U78, and U373) showed IC_{50} values greater than 1 μM. **HH33** was nearby equipotent to the reference drug doxorubicin in HepG2 cells and displayed a superior activity than doxorubicin in HeLa cells. Furthermore, the selectivity of **HH32** and **HH33** toward cancer cells was tested by investigating their anti-proliferative effects on normal cells (Fibroblast F180 and epithelial cell HME1) (Figures S1I and S1J). The two tested compounds demonstrated lower cytotoxicity against both normal fibroblast and epithelial cells indicated by higher IC_{50}s (>13 μM for **HH32** and >3.9 μM for **HH33**) compared to doxorubicin (<1.2 μM) (Table 1). To get more insight on the selectivity of **HH32** and **HH33** compounds, the selectivity index of both compounds was calculated and found to be superior in most of cancer cell lines than doxorubicin[28] (Table 2). Collectively, these results demonstrate that **HH32** and **HH33** have potent anti-proliferative activity against various types of cancer cells with low impact on normal cells.

To further investigate the safety profile of **HH32** and **HH33** compounds, the ADME-Tox properties of these compounds were assessed *in-silico* via the *Pre*ADMET web server (https://preadmet.bmdrc.kr/).[29,30] The calculated parameters (Caco-2 and %HIA) suggested a moderate to high possibility of intestinal absorption (Table 3) with a moderate to low blood-brain barrier penetration ability as suggested by their % BBB values. Moreover, **HH32** and **HH33** compounds are expected to exhibit a weak plasma protein binding as indicated by their % PPB values. Both compounds were predicted to exhibit some P-glycoprotein inhibitory activity. On the other hand, our compounds are predicted to exhibit no carcinogenic effects and medium inhibitory risk toward the *h*ERG (Ether-a-go-go Related Gene) channel (Table 3). The overall calculated ADME-tox parameters suggested a good safety profile for **HH32** and **HH33** compounds with high suitability for oral administration.

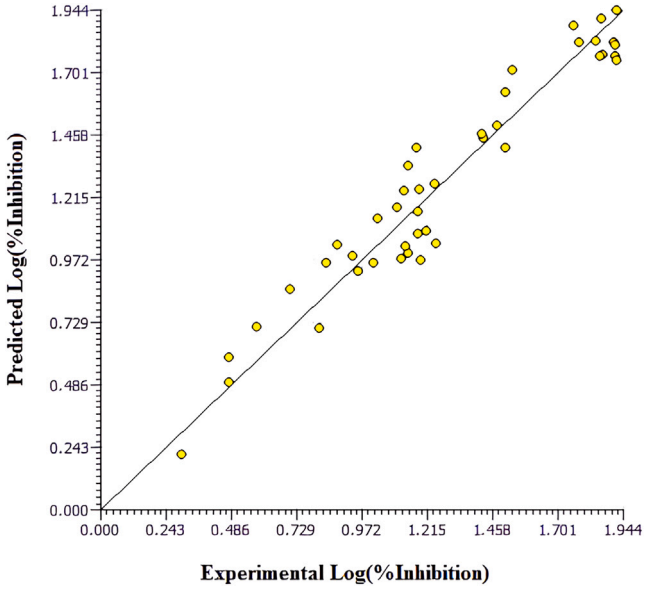

Figure 2. Scatterplot of Experimental versus predicted bioactivities (expressed by % inhibition against MCF7 cells) derived from the best QSAR equation

Downregulation of DNA repair and cell cycle progression pathways in HH33-treated cells

To get an insight into the mechanism of action and the possible pathways targeted by our compounds, transcriptomic analysis of the MCF7 (representing sensitive cells) and A549 (representing resistant cells) has been investigated after treatment with the **HH33** compound. **HH33** was selected because it showed better anti-proliferative activities than the **HH32**. Hypergeometric test of **HH33**-treated MCF7 cells showed the down-regulation of pathways related to DNA repair and cell cycle progression. (Figure 4A and Table S1). On the other hand, the treatment of A549 cells with HH33 induced an upregulation of the apoptotic signaling pathway and down-regulation of cell cycle progression pathway (Figures 4B, 4C, and Table S2). Of note, transcriptomics analysis of **HH33**-treated MCF7 and A549 cells showed six shared genes (*ATAD2*, *CDCA3*, *FAMIIIB*, *CDKN3*, *HISTIH2AH*, and *MIS18BP1*) that were maximally downregulated in both cell lines and were confirmed by quantitative RT-PCR (Figures 4D, S2, and Table S3). To validate the results of transcriptomic analysis, we studied the effect of **HH32** and **HH33** compounds on DNA damage induction, activation of DNA damage response machinery, effects on cell cycle progression, and induction of apoptosis.

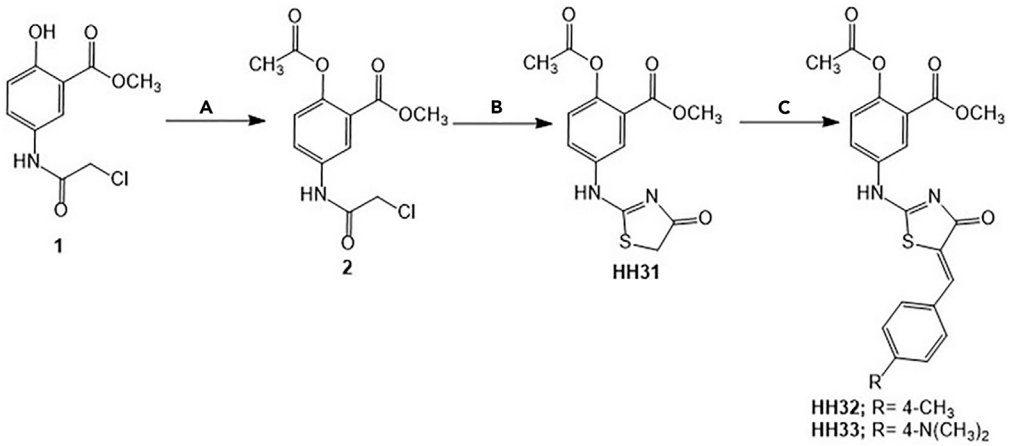

Scheme 1. Synthesis of the target compounds

Reagent and conditions: (A) Ac_2O, cat. H_2SO_4, rt 2 h, 92.5% yield; (B) NH_4SCN, CH_3CH_2OH, reflux 2 h, then at rt, overnight, 72% yield; (C) 4-methylbenzaldehde or 4-dimethylamio-benzaldehde, AcOH, AcONa, reflux, 24 h, 70-75% yield.

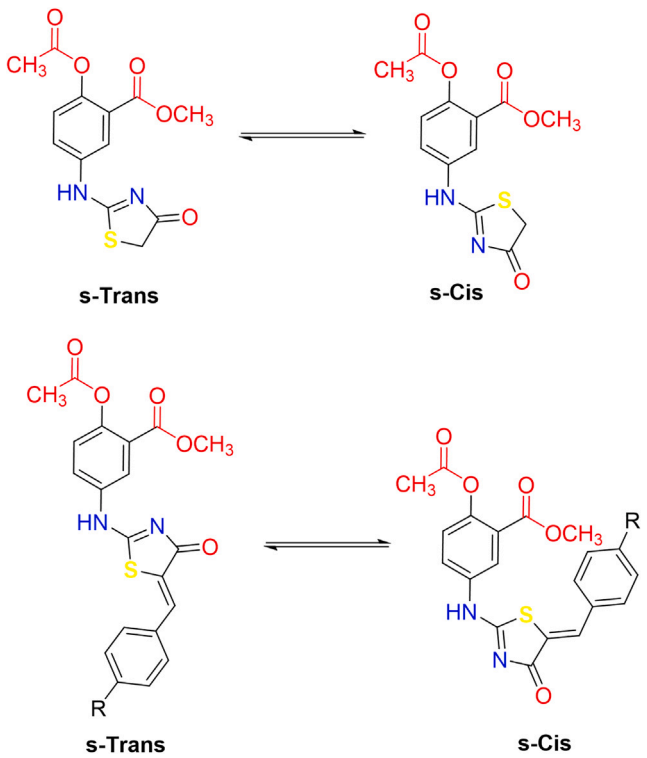

Figure 3. Syn/anti arrangement of rotamers of the cyclized compounds

HH32 and HH33 compounds as potent DNA damage inducers

The results of the transcriptomic analysis pointed out the ability of our compounds to target cellular DNA. To verify these results, we used neutral comet assay to detect the DNA damaging potential of our compounds in MCF7, HCT-116, and A549 cells. As shown in Figures 5A–5D, the level of DNA damage as indicated by the comet tail length and intensity (tail moment) was increased after treatment with **HH32** and **HH33** in a concentration-dependent manner in the three cell lines. Notably, comet length was markedly higher in **HH33**-treated cells than **HH32**-treated cells in both MCF7 and HCT-116 cells (Figures 5B and 5C). Interestingly, the level of DNA double strand

Table 1. Antiproliferative activities (IC_{50}) of HH32 and HH33 hybrids in comparison with Doxorubicin in cancer and normal cell lines

IC_{50} (μM) ± SEM[a]			
	HH32	HH33	DOX
MCF7	3.44 ± 0.32	0.81 ± 0.34	0.06 ± 0.38
HCT-116	1.17 ± 0.46	0.29 ± 0.47	0.11 ± 0.41
HeLa	0.60 ± 0.47	0.24 ± 0.51	0.46 ± 0.46
A549	6.17 ± 0.38	2.93 ± 0.83	0.62 ± 0.59
HepG2	2.49 ± 0.11	0.38 ± 0.11	0.37 ± 0.12
MDA-MB-231	15.35 ± 0.08	3.94 ± 0.08	0.45 ± 0.11
U87	6.53 ± 0.09	1.03 ± 0.11	0.10 ± 0.09
U373	29.38 ± 0.08	23.66 ± 0.08	0.88 ± 0.09
F-180[b]	13.34 ± 0.38	3.91 ± 0.43	0.29 ± 0.37
HME1[c]	26.79 ± 0.14	9.25 ± 0.14	1.12 ± 0.19

[a]Half maximal inhibitory concentration (IC_{50}) represents the concentration of compound corresponding to a survival fraction of 0.5. Represented data are means ± SEM of at least 3 independent experiments.
[b]Normal fibroblast cells.
[c]Normal mammary epithelial cells.

Table 2. Selectivity index of HH32 and HH33 compounds compared to selectivity index of Doxorubicin

	F180			HME1		
	HH32	HH33	Doxorubicin	HH32	HH33	Doxorubicin
MCF7	3.88	4.89	4.8	7.8	11.4	18.7
HCT116	11.4	13.48	2.6	22.9	31.9	10.2
HeLa	22.2	16.3	0.6	44.65	38.5	2.4
A549	2.16	1.3	0.47	4.3	3.2	1.81
HepG2	5.36	10.3	0.78	10.8	24	3.02
MDA-MB-231	0.87	0.99	0.64	1.7	2.3	2.5
U87	2.04	3.8	2.9	4.1	9	11.2
U373	0.45	0.17	0.33	0.9	0.4	1.3

Selectivity index was calculated by dividing the IC_{50} of the respective compound on the normal cells (F180 or HME1) by its IC_{50} on the cancer cells.

breaks induced by treatment with 1 μM of **HH33** was higher than doxorubicin treatment using the same concentration in the three tested cell lines. These results clearly demonstrated the capability of **HH32** and **HH33** to target the cellular DNA inducing extensive DNA damage.

DNA damage response machinery activation by HH32 and HH33 compounds

Induction of DNA damage activates a network of proteins called DNA damage response machinery (DDR). Phosphorylation of H2Ax histone in the area surrounding the damaged sites is an early event indicating DNA damage. Activation of the signal transducer kinases ATM and ATR is central to the DDR, which results in the phosphorylation and subsequent activation of downstream proteins such as ChK1, ChK2, p53, BRCA1/2 to stop cell cycling and to allow for DNA repair or for the activation of cell death pathways. Treatment of MCF7, HeLa, HCT116, and A549 cells with **HH32** and **HH33** compounds resulted in a marked elevation of the level of *p*-H2Ax (γ-H2Ax), a well-reported marker for DNA damage (Figures 6A–6D). In particular, **HH33** resulted in the higher elevation of the γ-H2Ax than the **HH32** compound (Figures 6A–6C). On the other hand, the two compounds did not induce the formation of γ-H2Ax in the A549 cell line indicating the low level of DNA damage and/or efficient DNA repair (Figure 6D). As

Table 3. Calculated ADME-Tox properties of HH32 and HH33 predicted via *Pre*ADMET server

ADME-Tox Property	HH32	HH33
BBB[a]	0.255	0.0546
HIA[b]	97.772	98.030
Caco-2[c]	14.879	17.782
log*kp*[d]	−3.396	−3.537
PPB[e]	89.602	89.259
Pgp[f]	*Positive* (+)	*Positive* (+)
CYP-2C19[g]	*Negative* (−)	*Negative* (−)
CYP-2C9	*Positive* (+)	*Positive* (+)
CYP-2D6	*Negative* (−)	*Negative* (−)
CYP-3A4	*Positive* (+)	*Negative* (−)
*h*ERG[h]	*Medium risk*	*Medium risk*
Carcinogen (Mouse)	*Negative* (−)	*Negative* (−)
Carcinogen (Rat)	*Negative* (−)	*Negative* (−)

[a]blood-brain barrier penetration (C. brain/C. blood): >2 high absorption to CNS; between 0.1 and 2 middle absorption to CNS, while <0.1 represents low absorption to CNS.
[b]percent human intestinal absorption: 0–20% poorly absorbed; 20–70% moderately absorbed, while 70–100% is well-absorbed.
[c]human colon adenocarcinoma permeability (nm/s): <4 low permeability; 4–70 middle permeability, while >70 considered of high permeability.
[d]skin permeability (cm/h) epercent plasma protein binding: >90% strongly bound; <90% weakly bound.
[f]P-glycoprotein inhibitory activity (related to multi-drug resistance).
[g]Cytochrome P-450 inhibitory activity.
[h]in-vitro Human ether-a-go-go related gene channel inhibition.

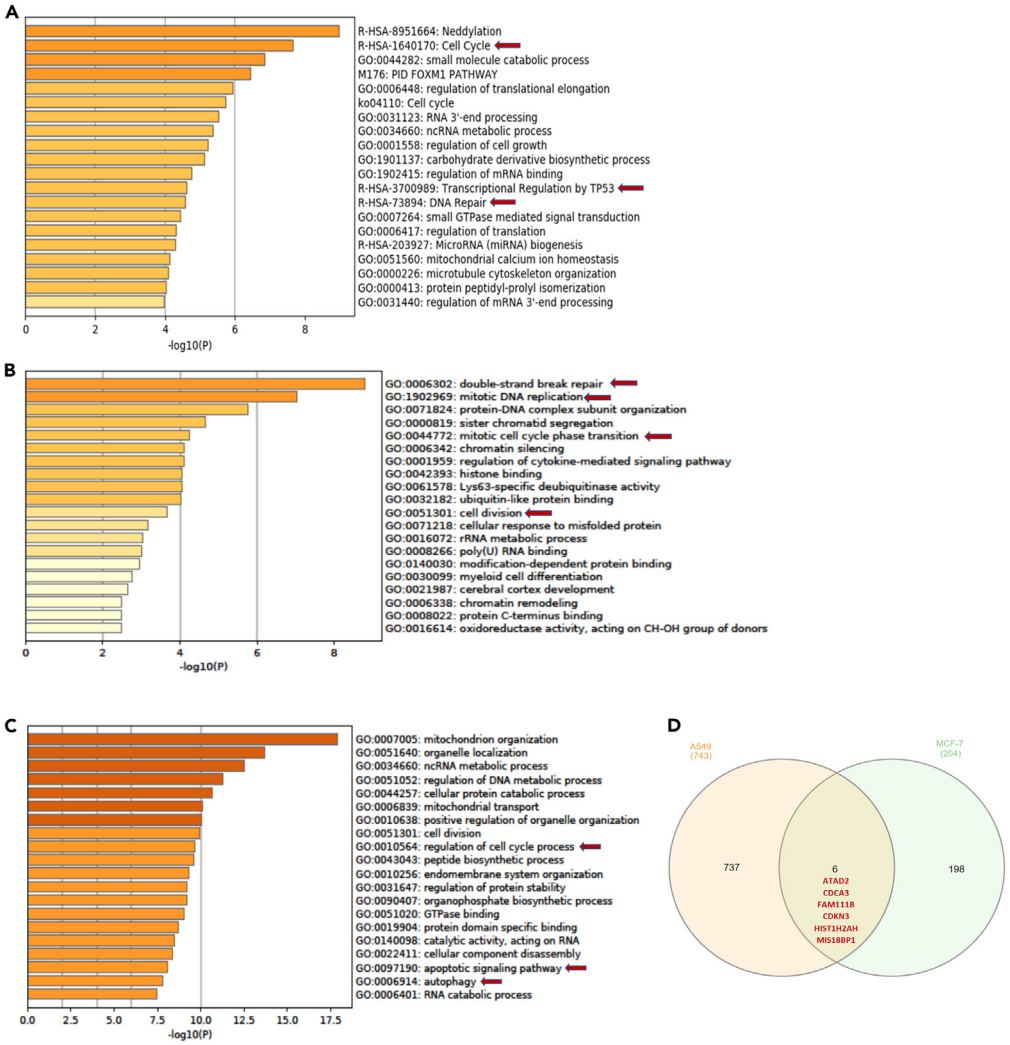

Figure 4. Transcriptomic analysis of HH33-treated MCF7 and A549 cells

(A) Hypergeometric test of the differentially expressed cellular pathways showing the downregulated pathways in **HH33**-treated MCF-7 cells (n = 3) compared to DMSO-treated cells (n = 3).

(B and C) Hypergeometric test of the differentially expressed cellular pathways showing the (B) downregulated and (C) upregulated pathways in **HH33**-treated A549 cells (n = 3) compared to DMSO-treated cells (n = 3). The analysis was done using metascape (http://metascape.org): a gene annotation and analysis online resource generating a graphical presentation, using gene onotology (GO) pathways.

(D) Venn diagram showing six shared maximally downregulated genes between **HH33**-treated MCF7 (n = 198) and A549 (n = 737) cells. See also Figure S2 and Tables S1–S3.

illustrated in Figure 6E, the phosphorylation status of ATM and its downstream target Chk2 increased significantly by **HH32** and **HH33** in MCF7, HCT-116 and A549 cells while only by **HH32** treatment in HeLa cells (Figures 6F–6H). Similar results were seen for the activation of ATR/Chk1 cascade under the same treatment conditions with **HH32** and **HH33** in the four cell lines (Figures 6I–6L). These data indicate that **HH32** and **HH33** induce DNA damage and activate ATM/Chk2 and ATR/Chk1 signaling pathways.

Cell-cycle arrest at the G2/M phase induced by HH32 and HH33 compounds

The cell growth inhibition and the induction of DNA damage are often linked to the dysregulation of cell cycle machinery. In this regard, we studied the effects of **HH32** and **HH33** on cell cycle distribution at various time intervals (Figures 7A–7D and S3). The two compounds induced a significant arrest of the cells at the G2/M phase in the four cell lines at different time points (Figures 7A–7D). In cells treated with 1μM of **HH33**, G2/M phase accumulation peaked at 8 h in HCT116 (Control 27.4%, **HH33** 77.4%) and at 24 h in HeLa cells (Control 36.9%, **HH33** 93.9%). On the other hand, treatment with **HH33** resulted in strong G2/M cell-cycle arrest in MCF7 and A549 cells in a time-dependent manner and it was maintained up to 72 h (MCF7: Control 11.3%, 1μM **HH33** 57.7%; A549: Control 8.5%, 1μM **HH33** 45.1%) (Figures 7A and 7D).

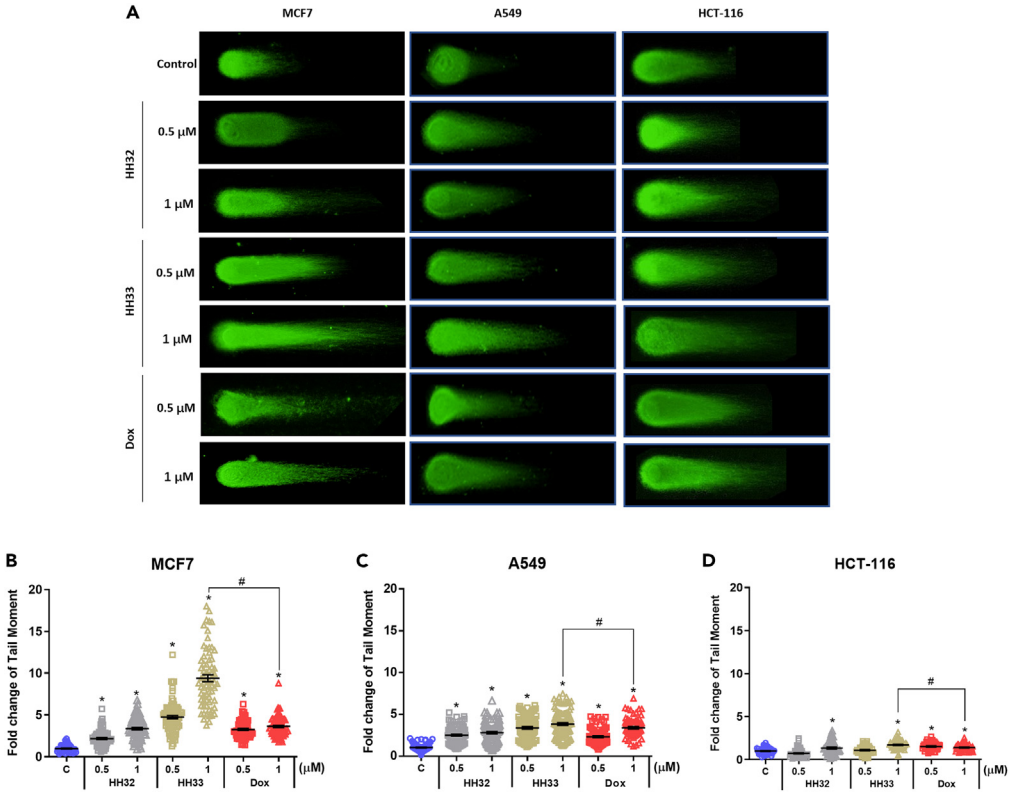

Figure 5. Induction of DNA damage by HH32 and HH33 in cancer cell lines

(A) Representative images of the neutral comet assay on MCF7, A549 and HCT-116 cells treated with 0.5 and 1 μM of **HH-32**, **HH-33** and Doxorubicin for 24 h. The cell appears like a comet with a head containing the intact DNA and a tail containing a damaged DNA.

(B–D) Graph for fold change of tail moment over control untreated cells in (B) MCF7, (C) A549 and (D) HCT-116. Each symbol represents a cell. Data presented as mean ± SEM; n = 3, unpaired Student's *t* test, *p < 0.05 vs. control (C). #p < 0.05 vs. 1 μM Dox.

Interestingly, the arrest of all cell lines in G2/M phases was accompanied with the appearance of a substantial sub-G1 cell population particularly in HCT116 and HeLa cells, reflecting the increase in DNA fragmentation, which indicates apoptotic cells (Figures 7E–7H). However, no signs of G1 and S phases arrest were observed in the four cell lines following **HH32** or **HH33** treatment (Figures S3A–S3D).

In agreement with the flow cytometry analysis of the cell cycle, **HH33** was more effective than **HH32** in reducing the expression of proteins involved in the G2/M phase progression (cyclin A, cyclin B, CDC25c, and CDC2/CDK1) (Figures 7I–7L and S4). On the other hand, the cyclins and cyclin-dependent kinases (cyclin E, cyclin D1, and CDK2), which are involved in G1-S phase transition, were slightly changed after **HH32** and **HH33** treatment (Figure S5). Moreover, we tested the anti-proliferative activity of **HH33** on CDK4 knockout HCT116 cells. Also, we checked for the effect of **HH33** on cell cycle progression in these knockout cells. Since CDK4 is known to be involved in regulating the passage of cells through G1 and S phases but not G2/M phases,[31,32] our results showed no difference neither in the sensitivity nor the cell cycle distribution between wild-type and CDK4 knockout cells after treatment with HH33 (Figure S6).

The function of the cyclin/cyclin-dependent kinase (CDK) complex in cell cycle progression is negatively regulated by CDK inhibitors such as p53 and p21, which were reported to contribute to G2/M phase arrest. Both **HH32** and **HH33** substantially increased the expression of p53 and p21 in MCF7, HCT-116, and A549 cells, while both markers were reduced in HeLa cells (Figures 7I–7P). Furthermore, we used two phospho-retinoblastoma (Rb) antibodies (ser-249 and ser807/811) to investigate the effects of our two compounds on the phosphorylation of Rb, which acts as a cell cycle control checkpoint. The two compounds induced a reduction in Rb phosphorylation (ser-249 and ser807/811) in MCF7 and A549 cells (Figures 7M–7P). However, the phospho-Rb (ser249) was increased in HCT116 and HeLa cells upon treatment with **HH32** and **HH33** compounds, while the phospho-Rb (ser807/811) was reduced in HCT-116 and increased in HeLa cells (Figures 7N and 7O). Taken together, **HH32** and **HH33** upregulated CDK inhibitors, downregulated G2/M progression markers and ultimately arrest the cells at the G2/M phase.

Molecular modeling and binding mode analysis of HH-32 and HH-33 to cell cycle regulators

The effects of **HH32** and **HH33** compounds on cell cycle progression and their ability to inhibit the expression of cell cycle proteins such as cyclins, CDKs, and phosphatases encouraged us to perform molecular docking simulations. This analysis was done to disclose the most probable binding modes of our compounds within such protein targets, and to provide explanations for their measured inhibitory effects. Overall,

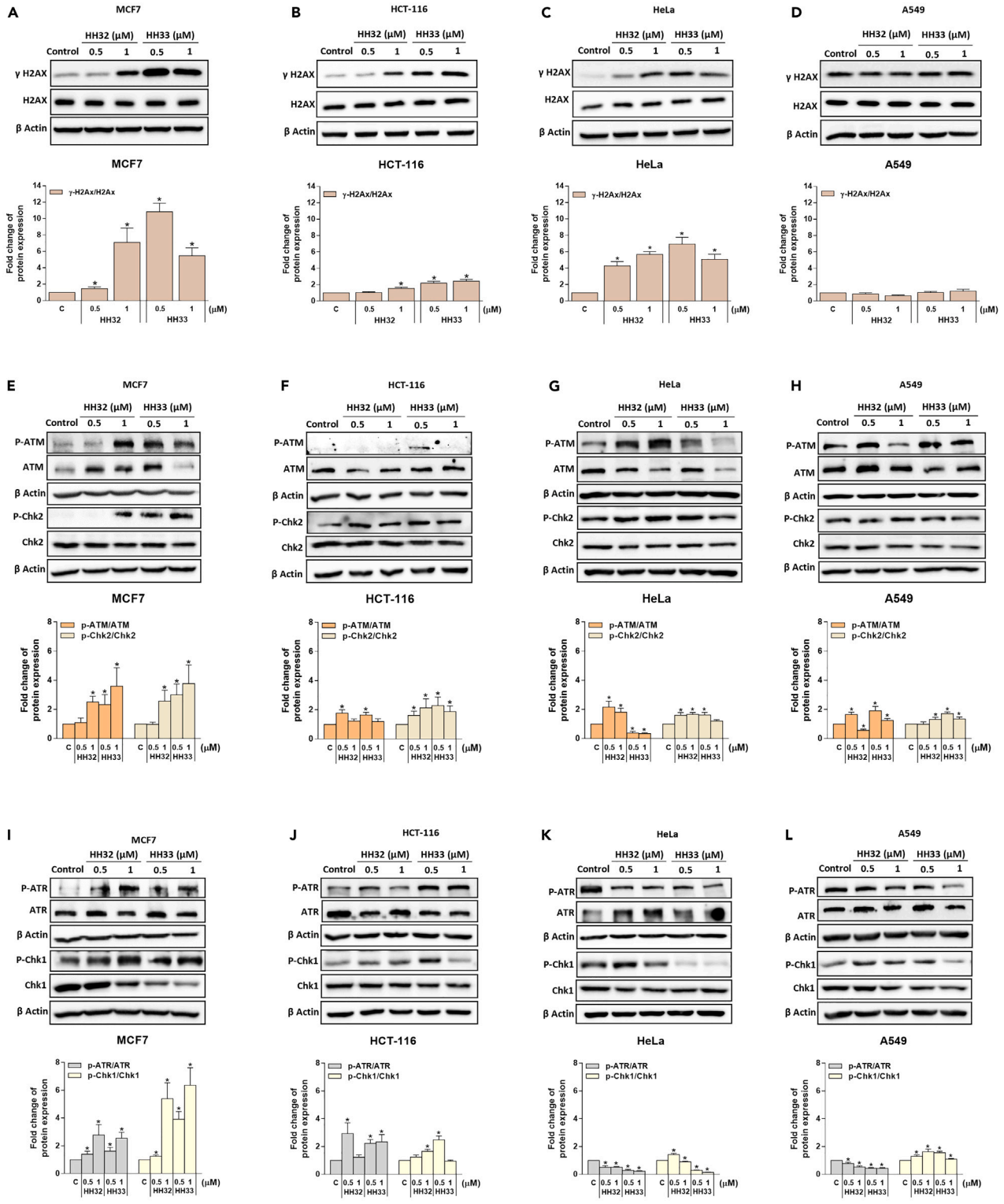
A
MCF7
HH32 (μM)
HH33 (μM)
Control 0.5 1 0.5 1
γ H2AX
H2AX
β Actin
MCF7
γ-H2Ax/H2Ax
Fold change of protein expression
C 0.5 1 0.5 1 (μM)
HH32 HH33
B
HCT-116
HCT-116
C
HeLa
HeLa
D
A549
A549
E
MCF7
P-ATM
ATM
β Actin
P-Chk2
Chk2
p-ATM/ATM
p-Chk2/Chk2
F
HCT-116
G
HeLa
H
A549
I
MCF7
P-ATR
ATR
P-Chk1
Chk1
p-ATR/ATR
p-Chk1/Chk1
J
HCT-116
K
HeLa
L
A549

Figure 6. DNA damage response induced after HH32 and HH33 treatment

(A–D) MCF7, HCT-116, HeLa and A549 were treated with 0.5 and 1 μM of **HH32** or **HH33** for 24h. Upper panels: Western blots detection for γ-H2AX following treatment with **HH32** and **HH33**. Lower panels: Fold change quantification of γ-H2AX over DMSO -treated control normalized to the β-actin as a loading control.

(E–H) Upper panels: Western blots detection for P-ATM, ATM, P- Chk2 and Chk2 after treatment with **HH32** and **HH33**. Lower panels: P-ATM and P-Chk2 band quantification after normalization to the total protein and the β-actin as a loading control.

(I–L) Upper panels: Western blots analysis for P-ATR, ATR, P- Chk1 and Chk1 post **HH32** and **HH33** treatment. Lower panels: Fold change for P-ATR and P-Chk1 after band quantification and normalization to the total protein and the β-actin as a loading control. Error bars represent SEM of three independent experiments. Data presented as mean ± SEM; n = 3, unpaired Student's *t* test, *p < 0.05 vs. control (C).

the results of the molecular docking study suggested a proper fit between our compounds (**HH32** & **HH33**) and the active sites of the studied cell cycle proteins (CDK1-cyclin B1, CDK2-cyclin A, CDC25C, and Rb) as indicated by their high binding affinity scores (Table 4).

Binding mode analysis of our compounds within the active site of CDC25C phosphatase showed significant interactions with residues of the c-terminal region containing the HCX_5R motif. Both compounds (**HH32** & **HH33**) shared a common binding pattern (Figure S7A and Table S4) in which the thiazolinone carbonyl oxygen was able to form the hydrogen bond with the residue Glu-382, while the 5-aminosalicylate arm was able to form two H-bond interactions with the respective Arg-417 and His-440 amino acid residues. The present binding mode would enable such compounds to block this small shallow active site and to prevent accessibility to the catalytic cysteine (Cys-377) residue. Furthermore, the binding pattern observed between our compounds and the CDK1-CyclinB complex (maturation promoting factor; MPF) showed high similarity in their interactions with the residues of the active site. The compound **HH32** was able to establish two hydrogen bonding through the 5-aminosalicylate arm moieties and the corresponding n-terminal residues; Glu-12 and Tyr-15, while another set of H-bond interactions were observed between its thiazolinone carbonyl oxygen and nitrogen with the corresponding hinge region residues; Glu-81 and Leu-83 (Figure S7B). On the other hand, compound **HH33** showed a similar network of interactions except that with the residue Glu-81 (Figure S7B).

The binding mode secured by our compounds with respect to the CDK2/CyclinA complex suggested a similar binding interactions pattern, in which, the 5-aminosalicylate arm was able to establish H-bond with the n-terminal residue (Lys-33), while the 5-aminosalicylate nitrogen was able to form significant H-bond with the hinge region residue (Leu-83). Finally, the thiazolinone carbonyl oxygen was able to form multiple H-bond interactions with the residue Asp-86 of the solvent exposed region (Figure S7C).

High binding affinities were observed between our compounds and the retinoblastoma tumor suppressor (pRb) protein E2F binding site. The compound HH32 was able to establish four H-bond interactions; one with the residue Lys-530 through its thiazolinone carbonyl oxygen, and another one with the helix α-4 residue Glu-464 through its 5-aminosalicylate nitrogen, while the remaining two were established between the 5-aminosalicylate arm moieties with the corresponding residues; Ser-463 and Lys-537 (Figure S7D). The compound **HH33** showed a similar network of interactions with an additional one with the residue Ser-534 (Figure S7D).

Apoptosis triggered by HH32 and HH33 through intrinsic and extrinsic pathways

To examine the mechanism of cell death of **HH32** and **HH33**, the detection of apoptotic and necrotic dead cells was performed by Annexin V and Propidium iodide (PI) double staining after 12-, 24- and 48-h treatment with **HH32** and **HH33** compounds (Figures 8A–8D and S8). The early apoptotic cell population (Annexin V+/PI-) of MCF7, HCT-116, HeLa, and A549 cells was increased after 24 and 48 h of **HH33** treatment (Figures 8A–8D). However, no sign of early apoptosis induction was detected following **HH32** treatment in the four cell lines. Notably, the population of late apoptotic/dead cells (Annexin V+/PI+) was increased with increasing the concentration of **HH33** in the four cell lines. This indicates that apoptosis is an important cell death mode induced particularly by **HH33** in the four cancer cell lines. It is well-known that the activation of apoptosis could be through mitochondria-mediated (intrinsic) or death-receptor (extrinsic) pathways.[33] The activation of the intrinsic apoptotic pathway was first tested and found to be induced by the **HH33** compound which was indicated by the increase in the cleavage of caspase-9 in MCF7, HeLa and A549 cells (Figures 8E–8H). Although the population of late apoptotic/dead cells (Annexin V+/PI+) was elevated by **HH32** and **HH33** in HCT-116 cells (Figure 8B), however, caspase-9 activation in HCT-116 cells was not induced by both compounds (Figure 8G). This suggests that the extrinsic pathway could also contribute to **HH32** and **HH33**-induced apoptosis which was examined by measuring the cleavage level of caspase-8 (Figures 8I–8L). In this regard, Western blot analysis showed that caspase-8 was cleaved by **HH32** and **HH33** in all cell lines and it was higher in cells treated with **HH33**. In addition, the cleavage of the downstream BID protein was induced also by both compounds in HCT-116, HeLa, and A549 cells (Figure 8J–8L). These results demonstrate that the observed death induced by **HH32** and **HH33** is through a caspase-dependent apoptotic pathway, which might involve both intrinsic and extrinsic pathways.

The effect of HH32 and HH33 treatment on the level of c-MYC protein

The anticancer activity of **HH32** and **HH33** was further investigated by measuring the expression of the oncogene c-Myc in the four cancer cell lines. Myc is a proto-oncogene and acting as a transcription factor that binds DNA and activates the transcription of growth-related genes.[34] Therefore, Western blot analysis was done for the effect of **HH32** and **HH33** treatment on total c-Myc protein level (Figure 9A). HH32-mediated downregulation of c-Myc was observed at 1 μM concentration in MCF7 and HCT-116 cells. While **HH33** treatment decreased c-Myc protein level in the four cancer cell lines at 0.5 and 1 μM concentrations (Figures 9A and 9B). These results indicate the downregulation of c-Myc protein by **HH32** and **HH33** in cancer cell lines.

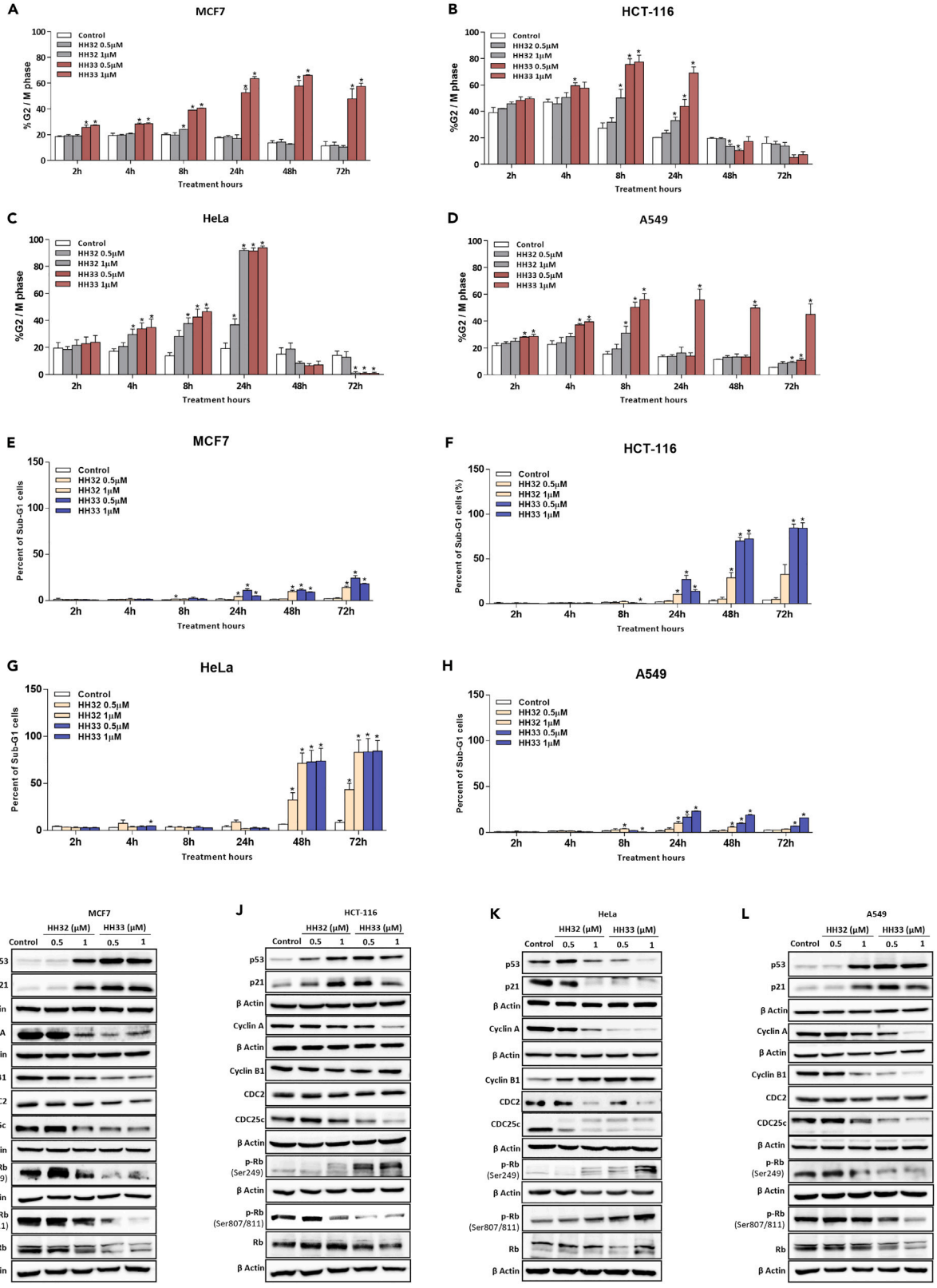
A
MCF7
B
HCT-116
C
HeLa
D
A549
E
MCF7
F
HCT-116
G
HeLa
H
A549
Control
HH32 0.5μM
HH32 1μM
HH33 0.5μM
HH33 1μM
%G2 / M phase
Percent of Sub-G1 cells
Percent of Sub-G1 cells (%)
Treatment hours
2h
4h
8h
24h
48h
72h
I
MCF7
J
HCT-116
K
HeLa
L
A549
HH32 (μM)
HH33 (μM)
Control
0.5
1
p53
p21
β Actin
Cyclin A
Cyclin B1
CDC2
CDC25c
p-Rb (Ser249)
p-Rb (Ser807/811)
Rb

Figure 7. HH32 and HH33 induce G2/M phase arrest accompanied with accumulation in the sub-G1 phase

(A–H) PI staining and cell cycle analysis using flow cytometry were performed after treatment with DMSO, 0.5 or 1 μM **HH32** or **HH33** for the indicated time points. (A–D) Bar Graphs showing the percentage of G2/M phase arrest after treatment. (E–H) Graphs showing the percentage of sub-G1 accumulation after treatment. See also Figure S3.

(I–L) Western blots analysis for p53, p21, Cyclin A, Cyclin B1, CDC2, CDC25c, p-Rb (Ser249), p-Rb (Ser807/811) and Rb proteins in the tested cells after treatment with 0.5 and 1 μM of **HH32** or **HH33** for 24 h. See also Figures S4–S6.

The metabolomic profile of cancer cells modulated by HH32 and HH33

Recent discoveries in the field of cancer cells metabolism are supporting the direction of considering cancer as a metabolic disease.[35,36] This opened the door for new cancer therapeutics that selectively targeting metabolic pathways altered during tumorigenesis. Accordingly, we tested the effects of the two compounds on the metabolomics of the MCF7 cells. Using the Human Metabolome Database (HMDB 4.0), a total of 53 metabolites was detected in MCF7 samples. Next, we investigated the effect of the drug treatment on each single metabolite using a Student's *t* test and the analysis revealed that Guanosine levels were altered after treatment with **HH32**. In addition, a significant decrease in the levels of Decanoic Acid, Adenosine, and 1-Monopalmitin was observed in cells treated with **HH33** as compared to untreated cells (Table S5). Interestingly, the analysis of 1-Monopalmitin level showed a 4.5-fold reduction in cells treated with **HH33** compared to control cells.

DISCUSSION

Selective reduction or inhibition of cancer cell proliferation is an important target of cancer therapeutics. Here, we developed acetyl-5-aminosalicylic acid and 4-thiazolinone derivatives (**HH32** and **HH33**) with anticancer activity (Figure 9C). One of the striking effects of our aminosalicylate-thiazolinone-based compounds, particularly the **HH33**, is the arrest of a very high percentage of cancer cells (up to 90%) at the G2/M border. This effect may be due to the induction of DNA damage by **HH33**, which modulates the expression or the activity of cell cycle regulatory proteins such as the p53, p21, cyclins, CDKs and phosphatases. A marked increase in the tail moments in the comet assay and in the level of γ-H2AX, markers of DNA damage, confirmed the induction of DNA damage by both compounds. Surprisingly, none of the two compounds induced neither G1/S nor intra S-phase arrest in any of the tested cell lines neither at short nor at long incubation periods. We speculate that the compounds induce replication-dependent DNA damage which activates the G2/M, but not the G1/S checkpoint.[37] Regulation of these cell cycle checkpoints (G1/S, intra-S, and G2/M) is achieved by different families of proteins including the cyclins, the CDKs and the CDK inhibitors.[38] Activation of the G2/M checkpoint subsequent to DNA damage induction is mainly initiated through activating the p53 protein which in turn activates its down-stream protein p21.[39] Active p21, by phosphorylation, inhibits the cyclin B/CDK1 complex and prevents cells from crossing the G2 border into the mitotic phase.[40] In line with the high percent of cells arrested at the G2 phase after treatment with **HH32** and **HH33** compounds, the levels of p53 and p21 were significantly increased, while the level of cyclin B1 and CDK1 was reduced in two out of the four tested cell lines (MCF7, and A549). The reduction of p53 and p21 levels and the increased level of cyclin B1 in HeLa cells under the same treatment conditions may be attributed to the abnormal status of p53 in these cells. Over 90% of cervical cancers and cancer-derived cell lines including HeLa contain inactivated p53, where the p53 tumor suppressor pathway is disrupted by human papillomavirus (HPV).[41]

Activation of the G2/M checkpoint after the induction of DNA damage aims at preventing the cells from entry into mitosis with damaged DNA.[42] This delay in cell cycle progression allows the cellular DNA repair machinery to repair the damaged DNA before progression to the mitosis which is the most critical phase of the cell cycle. If cells are defective in repairing the DNA damage or the damage is beyond the ability of the cells to repair, cell death pathways such as apoptosis are activated.[43] The G2 arrest induced by the two compounds and particularly by the **HH33** was sustainable in MCF7 and A549 cells during the whole investigation period (up to 72 h), while this G2 arrest reached peak at 24h in the other two cell lines (HCT116 and HeLa) and was greatly reduced at 48 and 72 h with the appearance of sub-G1 cells indicative of apoptosis. This indicates that the amount of DNA damage induced by the compounds at these concentrations was beyond the ability of the four cell lines to repair, but due to the different genetic backgrounds, two cell lines (MCF7 and A549) were not able to execute apoptosis and hence they were arrested at G2 phase for up to 72h. On the other hand, the other two cell lines (HCT116 and HeLa) underwent apoptosis after failure to repair the compounds-induced DNA damage, which may explain the high sensitivity of these two cell lines to the tested compounds.

Retinoblastoma (Rb) protein is one of the important players that has been previously reported to regulate the progression of the cell cycle.[44] Phosphorylation of the Rb at different sites by CDKs results in its inactivation and the release of E2F transcription factor, which in turns activates the transcription of genes required for the progression of the cell cycle such as the cyclins.[45] During the normal cell cycle

Table 4. Binding affinities of Doxorubicin, HH32 and HH33 against the studied molecular targets

	Docking Score (Kcal/mole)			
	CDC25C	CDK1-CyclinB	CDK2-CyclinA	Rb-Supressor
Doxorubicin	−7.4	−10.2	−9.9	−8.7
HH-32	−8.10	−11.50	−9.80	−10.10
HH-33	−8.00	−11.20	−9.60	−9.50

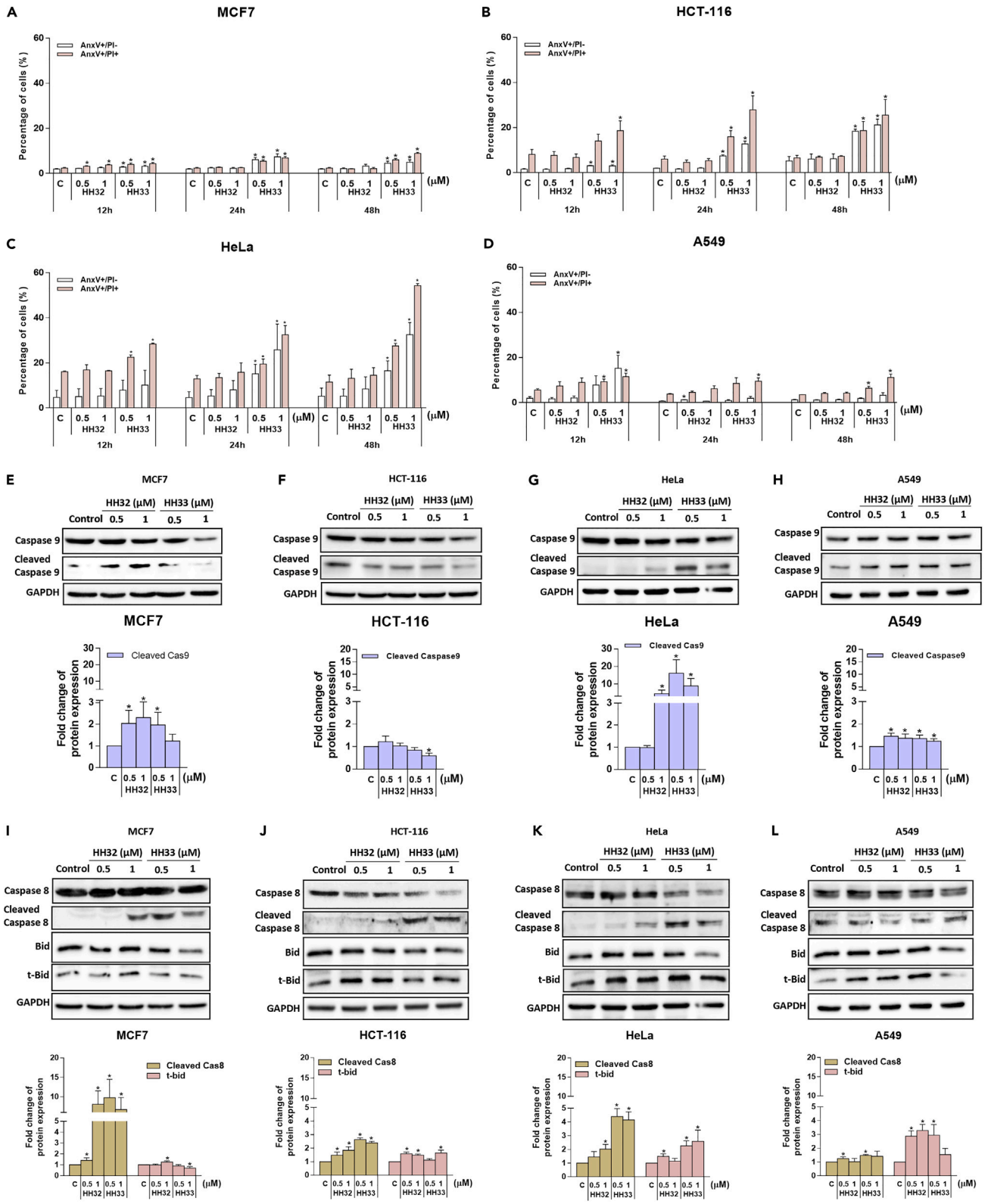
A
MCF7
B
HCT-116
C
HeLa
D
A549
AnxV+/PI-
AnxV+/PI+
Percentage of cells (%)
C
0.5
1
HH32
HH33
(μM)
12h
24h
48h
E
F
G
H
HH32 (μM)
HH33 (μM)
Control
Caspase 9
Cleaved Caspase 9
GAPDH
Cleaved Cas9
Cleaved Caspase9
Fold change of protein expression
I
J
K
L
Caspase 8
Cleaved Caspase 8
Bid
t-Bid
Cleaved Cas8
t-bid

Figure 8. Effect of HH32 and HH33 on intrinsic and extrinsic apoptotic pathways

(A–D) Cells were treated with 0.5 μM and 1 μM by **HH32** and **HH33** for 12, 24 and 48 h. Fluorescein-conjugated Annexin V and propidium iodide (PI) staining were used to measure the induction of apoptosis using flow cytometry. See also Figure S8.

(E–H) Upper panels: Western blot analysis for intrinsic apoptosis markers (expression/cleavage of caspase 9) in MCF7, HCT116, HeLa and A549 cells after treatment with 0.5 or 1 μM **HH32** or **HH33** for 24 h. Lower panels: bands intensities quantifications normalized to β-actin and DMSO-treated control.

(I–L) Upper panels: Western blot analysis for extrinsic apoptosis markers (expression/cleavage of caspase8 or bid) after treatment with 0.5 or 1 μM **HH32** or **HH33** for 24 h. Lower panels: bands intensities quantifications normalized to β-actin and DMSO-treated control. Data presented as mean ± SEM; n = 3, unpaired Student's *t* test, *p < 0.05 vs. control (C).

progression, Rb remains phosphorylated, which allows cell progression through G1, S, G2 and M phases. We used two phosphor-Rb antibodies (ser-249 and ser807/811) to investigate the effects of our two compounds on the phosphorylation of Rb. The two compounds induced reduction in the Rb phosphorylation in MCF7 and A549 cells which is in line with the persistent G2/M arrest in these two cell lines. The phosphor-Rb (ser249) was increased in HCT116 and HeLa cells upon treatment with **HH32** and **HH33** compounds, while the phospho-Rb (ser807/811) was reduced in HCT116 and increased in HeLa cells. This also explains the reduction in G2/M arrest in these two cell lines after 24h of treatment with **HH32** and **HH33**. The increased the phosphorylation of Rb in these two cell lines lead to the release of the E2F transcription factor which activates the expression of genes such as cyclins and CDKs leading to the abrogation of the G2/M arrest and progression of cells into mitosis. Because these cells enter mitosis with damaged DNA, they undergo apoptosis which was indicated by the increased fraction of the sub-G1 population. In support of this result, higher fractions of cells in early and late apoptosis were observed in HCT116 and HeLa cells compared to MCF7 and A549 cells after treatment with **HH32** and **HH33** followed by staining with annexin V/propidium iodide. These results indicate that our compounds are more potent against cells capable of executing apoptosis. In addition to the indirect induction of G2/M arrest due to DNA damage, we do not exclude the possibility of direct inhibitory effects of our compounds on drivers of the cell cycle progression. This possibility is supported by the results of the molecular modeling which suggest a proper fit between our compounds and CDK1-cyclin B1, CDK2-cyclin A, CDC25C, and Rb.

Predicting the mode of action of the new compounds was derived by the results of the transcriptomic analysis. In addition to the differentially expressed pathways, we identified six genes that were shared among the most downregulated pathways in the MCF7 and A549 cells. Three (*ATAD2, CDCA3,* and *FAM111B*) out of these 6 genes are directly involved in the cell division and progression of the cell cycle. 1) *ATAD2* is a member of the AAA domain-containing protein 2 family of ATPase. It's a transcriptional coactivator of the nuclear receptor ESR1 that is needed to express a subset of estradiol target genes including *CCND1*, *MYC*, and *E2F*. *ATAD2* may be involved in the recruitment or occupancy of *CREBBP* at the promoters of several *ESR1* target genes. This protein is likely to be required for histone Hyperacetylation. It is involved in the estrogen-induced cell proliferation and cell cycle progression of breast cancer cells.[46] 2) *CDCA3*, or cell division cycle-associated protein-3, is an F-box-like protein that is involved in driving the entry of the cell into mitosis. *CDCA3* mediates the ubiquitination and degradation of WEE1 kinase at G2/M phase.[47] 3) *FAM111B* is highly expressed in tumor tissues compared with normal tissues. Overexpression of *FAM111B* promoted the growth of lung cancer cells through a direct effect on p53 and influencing the expression of BAG3 and BCL2.[48]

Upregulated machinery of lipid metabolism has been observed in cancer cells to allow the formation of the cell membrane required for the rapidly dividing cells, whereas mitotically arrested and apoptotic cells were shown to have high accumulation of lipid droplets following treatment with chemotherapeutic drugs.[49] This may help the cancer cells to overcome the effects of anti-cancer agents and may contribute to the development of resistance. Interestingly, increased lipid droplet number is a feature of aggressive breast cancer.[50] However, targeting fatty acid (FA) metabolism was not generally identified as a potential therapeutic approach in cancer, due to the high plasticity of the FA metabolic pathways, yet it remains an additional desirable effect of anticancer therapy.[51] Therefore, the present study involved analyzing the release of different metabolites following **HH32** and **HH33** treatment. We report here a 4.5-fold reduction in the level of 1-monopalmitine in **HH33**-treated MCF7 cells compared to control cells. 1-Monopalmitin, which is a monoacylglycerol (MAG), is formed via the release of fatty acid from diacyglecerol (DAG) by DAG lipase. This may indicate the reduced hydrolysis of DAG (may be due to the inhibition of DAG lipase by **HH33**; or due to the inhibition of Fatty acid synthase (FASN), the rate-limiting enzyme in FA synthesis, or stearoyl-CoA desaturase (SCD); the unsaturation enzyme that convers palmitate into mono-palmitin), with the subsequent deprivation of the MCF7 cells of an important source of energy, which contribute to the anti-proliferative activity of **HH33**.

Noteworthy, especially under metabolic stress, cancer cells acquire various mechanisms to enhance exogenous FA uptake, a fact that minimizes the importance of FASN as an anti-cancer target.[52,53] In our metabolomic study, palmitic acid was significantly increased at 20% in **HH33**-treated MCF7 cells, denoting that the FASN was not suppressed. Moreover, the **HH33**-induced reduction in the level of decanoic acid in MCF7 cells may also indicate a lipolytic-inhibitory effect of **HH33**, which deprives the cancer cells of an important source of energy and structural fats needed for their proliferation. An earlier study has proposed a role for decanoic acid in stimulating *de novo* lipogenesis in cancer cell (e.g.,.U87MG cells) by a PPARγ-mediated mechanism.[54] Pharmacological inhibition of fatty acid synthesis is reported to be selectively cytotoxic to cancer cells *in vivo* and *in vitro*.[55] Moreover, a significant reduction of adenosine, an endogenous substance, in **HH33**-treated MCF7 cells was observed in metabolic analysis. For instance, adenosine is involved in many cellular processes including neurotransmission, regulation of cellular growth, metabolism and immune checkpoint.[56,57] Accumulation of adenosine has been reported recently to be associated with tumor progression and the ability of cancer cells to escape from the host immune.[58] These results indicate the ability of **HH33** to reduce the synthesis of adenosine or to enhance its degradation, which shed light on other effects of our derivatives that may support their use in combination with immunotherapy.

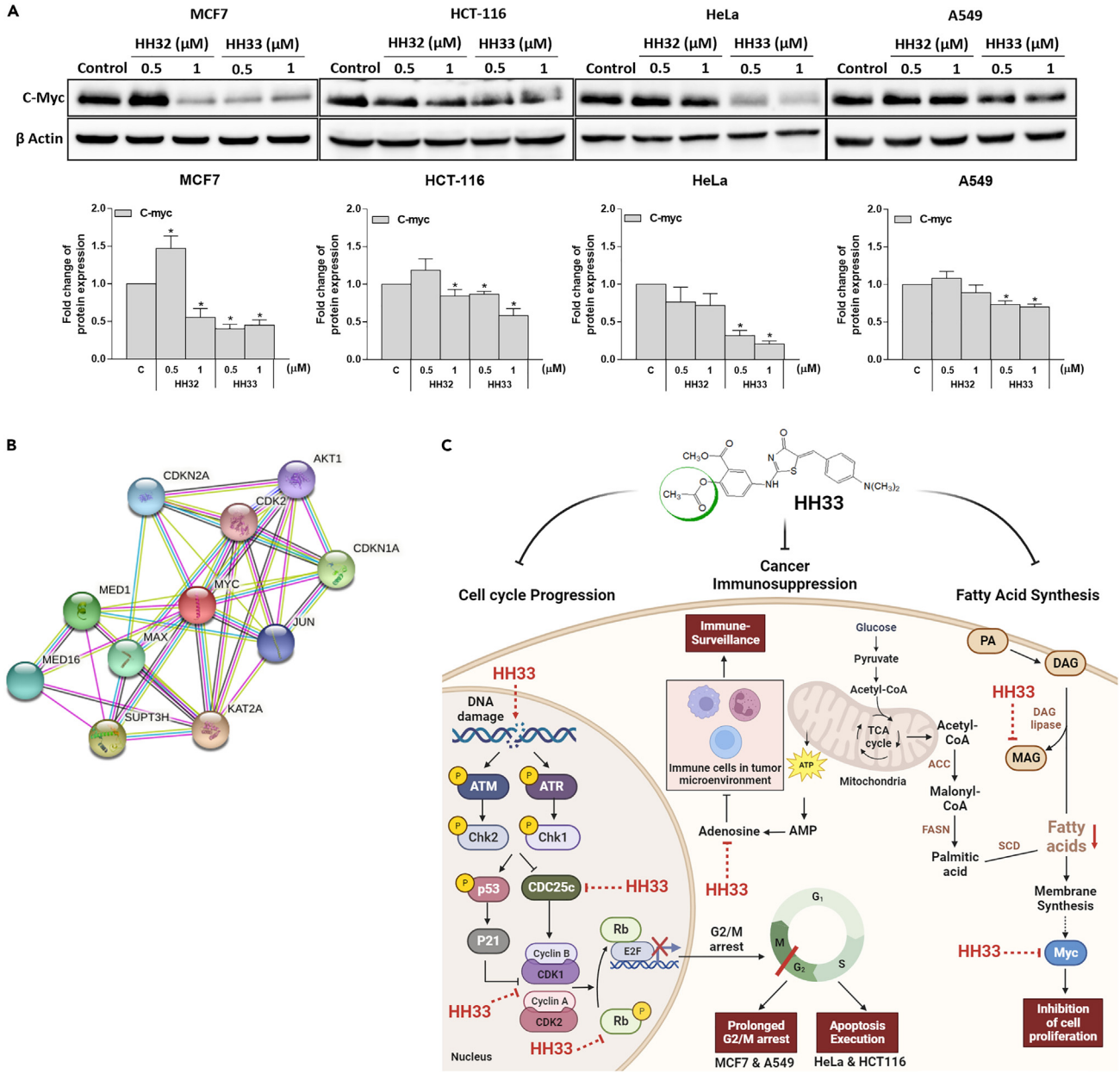

Figure 9. Effect of HH32 and HH33 on c-Myc expression

(A) Upper panel: Western blot analysis of c-Myc expression in MCF7, HCT-116, HeLa, and A549 cells following 24h treatment with 0.5 and 1μM of **HH32** and **HH33**. Lower panel: Band quantification of c-Myc expression in the indicated cell lines using β-actin as a loading control. Data presented as mean ± SEM; n = 3, unpaired Student's *t* test, *p < 0.05 vs. control (C).

(B) c-Myc network (using STRING functional protein association network).

(C) Schematic model for the mechanism of action of acetylated 5-aminosalicylate-4-thiazolinone derivative **HH33** in inhibiting cancer cell cycle progression, cancer immunosuppression and fatty acid synthesis which subsequently lead to cell death. PA, phosphatic acid; DAG, diacylglycerol; MAG, Monoacylglycerol; SCD, Stearoyl-CoA desaturase; ACC, Acetyl-CoA carboxylase; FASN, Fatty acid synthase; TCA cycle, citric acid cycle; AMP, Adenosine 5′-monophosphate; Rb, Retinoblastoma.

In conclusion, we described the anticancer activity of two new acetylated 5-aminosalicylate-4-thiazolinone derivatives (**HH32** and **HH33**) in a panel of cell lines from different tumor origin. These derivatives exerted an anti-proliferative activity through inducing DNA damage, G2/M cell-cycle arrest, and apoptosis. In addition, **HH32** and **HH33** compounds modulate the metabolic profile of cancer cells. Future study is needed to validate the cell cycle regulators as molecular targets of the hybrid compounds **HH32** and **HH33**. Additionally, further investigation is warranted to preclinically evaluate **HH32** and **HH33** compounds as an anticancer drugs using animal model bearing cancer cells.

Limitations of the study

Future study is needed to identify the exact targets of the hybrid compounds HH32 and HH33. Our structural data predicts the binding of HH32 and HH33 to Rb, CDK2-cyclinA, CDK1-cyclinB and Cdc25C. In addition, we showed that these derivatives downregulate the expression of these cell cycle regulators. However, it is unclear if these regulators are the direct targets of HH32 and HH33 to exert their anticancer activities. Although theses derivatives showed a better selectivity index than the anti-cancer drug doxorubicin, the safety of these compounds has not been tested in an *in vivo* setting. Additionally, the preclinical evaluation of HH32 and HH33 compounds as an anticancer drugs using nude mice bearing cancer cells has not been done in the study.

STAR★METHODS

Detailed methods are provided in the online version of this paper and include the following:

- KEY RESOURCES TABLE
- RESOURCE AVAILABILITY
  - Lead contact
  - Materials availability
  - Data and code availability
- EXPERIMENTAL MODEL AND STUDY PARTICIPANT DETAILS
  - Cell lines and culture conditions
- METHOD DETAILS
  - Design of new 5-**ASA**-thiazolinone derivatives
  - Quantitative structure-activity relationship (QSAR)
  - Synthesis of acetylated 5-ASA-thiazolinone derivatives HH32 and HH33
  - HH32 and HH33 compounds preparation
  - Cytotoxicity assay
  - Transcriptomic analysis
  - Western blot
  - Neutral comet assay
  - Cell cycle analysis
  - Apoptosis analysis
  - Molecular docking studies
  - Metabolic analysis
- QUANTIFICATION AND STATISTICAL ANALYSIS

SUPPLEMENTAL INFORMATION

Supplemental information can be found online at https://doi.org/10.1016/j.isci.2023.108659.

ACKNOWLEDGMENTS

The authors would like to express their gratitude to Professor Paola Gramatica for providing the licensed software. This work was financially supported by a collaborative project funded by the University of Sharjah and the Sharjah Research Academy, project number 2101110354. The CDK4 knockout experiment was funded by the MBRU-AlMahmeed Research Award 2019 (ALM1914).

AUTHOR CONTRIBUTIONS

R.E. conceptualized the study. W.S.R., H.H.M.A., M.H.S., A.A.E., N.C.S., T.V., R.H., S.H., and S.A. performed the experiments. W.S.R., H.T. and M.S.A. carried out the formal analysis and investigations. R.E., W.S.R., and M.S.A. wrote the original draft. E.S., A.A.E. and M.H.S. reviewed and edited the final article. R.E., W.S.R., and M.S.A. obtained funding. R.E., N.C.S., and R.H. provided resources for the study. R.E. supervised the study.

DECLARATION OF INTERESTS

The authors declare no competing interests.

A patent application for the two compounds described in this article has been submitted.

INCLUSION AND DIVERSITY

We support inclusive, diverse, and equitable conduct of research.

Received: September 18, 2023
Revised: October 29, 2023
Accepted: December 4, 2023
Published: December 9, 2023

REFERENCES

1. Singh, A.K., Kumar, A., Singh, H., Sonawane, P., Paliwal, H., Thareja, S., Pathak, P., Grishina, M., Jaremko, M., Emwas, A.H., et al. (2022). Concept of Hybrid Drugs and Recent Advancements in Anticancer Hybrids. Pharmaceuticals *15*, 1071.
2. Şahin, İ., Çeşme, M., Yüce, N., and Tümer, F. (2023). Discovery of new 1,4-disubstituted 1,2,3-triazoles: in silico ADME profiling, molecular docking and biological evaluation studies. J. Biomol. Struct. Dyn. *41*, 1988–2001.
3. Çot, A., Çeşme, M., Onur, S., Aksakal, E., Şahin, İ., and Tümer, F. (2023). Rational design of 1,2,3-triazole hybrid structures as novel anticancer agents: synthesis, biological evaluation and molecular docking studies. J. Biomol. Struct. Dyn. *41*, 6857–6865.
4. Şahin, İ., Çeşme, M., Özgeriş, F.B., and Tümer, F. (2023). Triazole based novel molecules as potential therapeutic agents: Synthesis, characterization, biological evaluation, in-silico ADME profiling and molecular docking studies. Chem. Biol. Interact. *370*, 110312.
5. Ekinci, D., Sentürk, M., and Küfrevioğlu, Ö.İ. (2011). Salicylic acid derivatives: synthesis, features and usage as therapeutic tools. Expert Opin. Ther. Pat. *21*, 1831–1841.
6. Tripathi, A.C., Gupta, S.J., Fatima, G.N., Sonar, P.K., Verma, A., and Saraf, S.K. (2014). 4-Thiazolidinones: the advances continue. Eur. J. Med. Chem. *72*, 52–77.
7. Senkiv, J., Finiuk, N., Kaminskyy, D., Havrylyuk, D., Wojtyra, M., Kril, I., Gzella, A., Stoika, R., and Lesyk, R. (2016). 5-Ene-4-thiazolidinones induce apoptosis in mammalian leukemia cells. Eur. J. Med. Chem. *117*, 33–46.
8. Teli, G., Sharma, P., and Chawla, P.A. (2023). Exploring the Potential of Substituted 4-Thiazolidinone Derivatives in the Treatment of Breast Cancer: Synthesis, Biological Screening and In Silico Studies. Polycycl. Aromat. Comp. *43*, 6202–6234.
9. Negi, M., Chawla, P., Faruk, A., and Chawla, V. (2022). The Role of 4-Thiazolidinone Scaffold in Targeting Variable Biomarkers and Pathways Involving Cancer. Anti Cancer Agents Med. Chem. *22*, 1458–1477.
10. Kumar, H., Kumar, D., Kumar, P., Thareja, S., Marwaha, M.G., Navik, U., and Marwaha, R.K. (2022). Synthesis, biological evaluation and in-silico ADME studies of novel series of thiazolidin-2,4-dione derivatives as antimicrobial, antioxidant and anticancer agents. BMC Chem. *16*, 68.
11. Chawla, P., Kalra, S., Kumar, R., Singh, R., and Saraf, S.K. (2019). Novel 2-(substituted phenyl Imino)-5-benzylidene-4-thiazolidinones as possible non-ulcerogenic tri-action drug candidates: synthesis, characterization, biological evaluation And docking studies. Med. Chem. Res. *28*, 340–359.
12. S Ramadan, W., Saleh, E.M., Menon, V., Vazhappilly, C.G., Abdu-Allah, H.H.M., El-Shorbagi, A.-N.A., Mansour, W., and El-Awady, R. (2020). Induction of DNA damage, apoptosis and cell cycle perturbation mediate cytotoxic activity of new 5-aminosalicylate–4-thiazolinone hybrid derivatives. Biomed. Pharmacother. *131*, 110571.
13. Abdu-Allah, H.H.M., Abdel-Moty, S.G., El-Awady, R., and El-Shorbagi, A.N.A. (2016). Design and synthesis of novel 5-aminosalicylate (5-ASA)-4-thiazolinone hybrid derivatives with promising antiproliferative activity. Bioorg. Med. Chem. Lett. *26*, 1647–1650.
14. Mahdi, J.G. (2010). Medicinal potential of willow: A chemical perspective of aspirin discovery. J. Saudi Chem. Soc. *14*, 317–322.
15. Hannah, J., Ruyle, W.V., Jones, H., Matzuk, A.R., Kelly, K.W., Witzel, B.E., Holtz, W.J., Houser, R.A., Shen, T.Y., and Sarett, L.H. (1978). Novel analgesic-antiinflammatory salicylates. J. Med. Chem. *21*, 1093–1100.
16. Collier, H.O.J. (1970). A Pharmacological Analysis of Aspirin. In Advances in Pharmacology, S. Garattini, A. Goldin, F. Hawking, and I.J. Kopin, eds. (Academic Press), pp. 333–405.
17. Rainsford, K.D., Schweitzer, A., and Brune, K. (1983). Distribution of the acetyl compared with the salicyl moiety of acetylsalicylic acid. Acetylation of macromolecules in organs wherein side-effects are manifest. Biochem. Pharmacol. *32*, 1301–1308.
18. Pinckard, R.N., Hawkins, D., and Farr, R.S. (1968). In vitro Acetylation of Plasma Proteins, Enzymes and DNA by Aspirin. Nature *219*, 68–69.
19. Lai, T.S., Davies, C., and Greenberg, C.S. (2010). Human tissue transglutaminase is inhibited by pharmacologic and chemical acetylation. Protein Sci. *19*, 229–235.
20. Alfonso, L.F., Srivenugopal, K.S., Arumugam, T.V., Abbruscato, T.J., Weidanz, J.A., and Bhat, G.J. (2009). Aspirin inhibits camptothecin-induced p21CIP1 levels and potentiates apoptosis in human breast cancer cells. Int. J. Oncol. *34*, 597–608.
21. Ai, G., Dachineni, R., Kumar, D.R., Marimuthu, S., Alfonso, L.F., and Bhat, G.J. (2016). Aspirin acetylates wild type and mutant p53 in colon cancer cells: identification of aspirin acetylated sites on recombinant p53. Tumour Biol. *37*, 6007–6016.
22. Chen, Z., Li, W., Qiu, F., Huang, Q., Jiang, Z., Ye, J., Cheng, P., Low, C., Guo, Y., Yi, X., et al. (2018). Aspirin cooperates with p300 to activate the acetylation of H3K9 and promote FasL-mediated apoptosis of cancer stem-like cells in colorectal cancer. Theranostics *8*, 4447–4461.
23. Ai, G., Dachineni, R., Kumar, D.R., Alfonso, L.F., Marimuthu, S., and Bhat, G.J. (2016). Aspirin inhibits glucose-6-phosphate dehydrogenase activity in HCT 116 cells through acetylation: Identification of aspirin-acetylated sites. Mol. Med. Rep. *14*, 1726–1732.
24. Comer, S.D., Sullivan, M.A., Whittington, R.A., Vosburg, S.K., and Kowalczyk, W.J. (2008). Abuse liability of prescription opioids compared to heroin in morphine-maintained heroin abusers. Neuropsychopharmacology *33*, 1179–1191.
25. Sassi, N., Mattarei, A., Azzolini, M., Bernardi, P., Szabo, I., Paradisi, C., Zoratti, M., and Biasutto, L. (2014). Mitochondria-targeted resveratrol derivatives act as cytotoxic pro-oxidants. Curr. Pharmaceut. Des. *20*, 172–179.
26. Vazhappilly, C.G., Saleh, E., Ramadan, W., Menon, V., Al-Azawi, A.M., Tarazi, H., Abdu-Allah, H., El-Shorbagi, A.N., and El-Awady, R. (2019). Inhibition of SHP2 by new compounds induces differential effects on RAS/RAF/ERK and PI3K/AKT pathways in different cancer cell types. Invest. N. Drugs *37*, 252–261.
27. Abdu-Allah, H.H.M., Abdelmoez, A.A.B., Tarazi, H., El-Shorbagi, A.-N.A., and El-Awady, R. (2020). Conjugation of 4-aminosalicylate with thiazolinones afforded non-cytotoxic potent in vitro and in vivo anti-inflammatory hybrids. Bioorg. Chem. *94*, 103378.
28. Kuete, V., Omosa, L.K., Tala, V.R.S., Midiwo, J.O., Mbaveng, A.T., Swaleh, S., Karaosmanoğlu, O., and Sivas, H. (2016). Cytotoxicity of Plumbagin, Rapanone and 12 other naturally occurring Quinones from Kenyan Flora towards human carcinoma cells. BMC Pharmacol. Toxicol. *17*, 60.
29. Lee, S.K., Lee, I.K., Chung, J.E., Sung, K.Y., and No, K.T. (2004). The PreADME: PC-Based Program for Batch Prediction of ADME Properties. EuroQSAR.
30. Lee, S.K., Kim, H.J., Chang, G.S., Chung, J.E., and No, K.T. (2003). The PreADME Approach: Web-Based Program for Rapid Prediction of Physico-Chemical, Drug Absorption and Drug-like Properties. EuroQSAR 2002 Designing Drugs and Crop Protectants: Processes, Problems and Solutions (Blackwell Publishing).
31. Neizer-Ashun, F., and Bhattacharya, R. (2021). Reality CHEK: Understanding the biology and clinical potential of CHK1. Cancer Lett. *497*, 202–211.
32. Chohan, T.A., Qayyum, A., Rehman, K., Tariq, M., and Akash, M.S.H. (2018). An insight into the emerging role of cyclin-dependent kinase inhibitors as potential therapeutic agents for the treatment of advanced cancers. Biomed. Pharmacother. *107*, 1326–1341.
33. Elmore, S. (2007). Apoptosis: a review of programmed cell death. Toxicol. Pathol. *35*, 495–516.
34. Gabay, M., Li, Y., and Felsher, D.W. (2014). MYC activation is a hallmark of cancer initiation and maintenance. Cold Spring Harb. Perspect. Med. *4*, a014241.
35. Stine, Z.E., Schug, Z.T., Salvino, J.M., and Dang, C.V. (2022). Targeting cancer metabolism in the era of precision oncology. Nat. Rev. Drug Discov. *21*, 141–162.
36. Martinez-Outschoorn, U.E., Peiris-Pagés, M., Pestell, R.G., Sotgia, F., and Lisanti, M.P. (2017). Cancer metabolism: a therapeutic perspective. Nat. Rev. Clin. Oncol. *14*, 11–31.
37. Willis, N., and Rhind, N. (2009). Regulation of DNA replication by the S-phase DNA damage checkpoint. Cell Div. *4*, 13.
38. Barnum, K.J., and O'Connell, M.J. (2014). Cell cycle regulation by checkpoints. Methods Mol. Biol. *1170*, 29–40.

39. Taylor, W.R., and Stark, G.R. (2001). Regulation of the G2/M transition by p53. Oncogene *20*, 1803–1815.
40. Dash, B.C., and El-Deiry, W.S. (2005). Phosphorylation of p21 in G2/M promotes cyclin B-Cdc2 kinase activity. Mol. Cell Biol. *25*, 3364–3387.
41. Hietanen, S., Lain, S., Krausz, E., Blattner, C., and Lane, D.P. (2000). Activation of p53 in cervical carcinoma cells by small molecules. Proc. Natl. Acad. Sci. USA *97*, 8501–8506.
42. Gatei, M., Sloper, K., Sorensen, C., Syljuäsen, R., Falck, J., Hobson, K., Savage, K., Lukas, J., Zhou, B.B., Bartek, J., and Khanna, K.K. (2003). Ataxia-telangiectasia-mutated (ATM) and NBS1-dependent phosphorylation of Chk1 on Ser-317 in response to ionizing radiation. J. Biol. Chem. *278*, 14806–14811.
43. Norbury, C.J., and Zhivotovsky, B. (2004). DNA damage-induced apoptosis. Oncogene *23*, 2797–2808.
44. Henley, S.A., and Dick, F.A. (2012). The retinoblastoma family of proteins and their regulatory functions in the mammalian cell division cycle. Cell Div. *7*, 10.
45. Giacinti, C., and Giordano, A. (2006). RB and cell cycle progression. Oncogene *25*, 5220–5227.
46. Hussain, M., Zhou, Y., Song, Y., Hameed, H.M.A., Jiang, H., Tu, Y., and Zhang, J. (2018). ATAD2 in cancer: a pharmacologically challenging but tractable target. Expert Opin. Ther. Targets *22*, 85–96.
47. Uchida, F., Uzawa, K., Kasamatsu, A., Takatori, H., Sakamoto, Y., Ogawara, K., Shiiba, M., Tanzawa, H., and Bukawa, H. (2012). Overexpression of cell cycle regulator CDCA3 promotes oral cancer progression by enhancing cell proliferation with prevention of G1 phase arrest. BMC Cancer *12*, 321.
48. Sun, H., Liu, K., Huang, J., Sun, Q., Shao, C., Luo, J., Xu, L., Shen, Y., and Ren, B. (2019). FAM111B, a direct target of p53, promotes the malignant process of lung adenocarcinoma. OncoTargets Ther. *12*, 2829–2842.
49. Vacek, L., Dvorak, A., Bechynska, K., Kosek, V., Elkalaf, M., Trinh, M.D., Fiserova, I., Pospisilova, K., Slovakova, L., Vitek, L., et al. (2022). Hypoxia Induces Saturated Fatty Acids Accumulation and Reduces Unsaturated Fatty Acids Independently of Reverse Tricarboxylic Acid Cycle in L6 Myotubes. Front. Endocrinol. *13*, 663625.
50. Antalis, C.J., Arnold, T., Rasool, T., Lee, B., Buhman, K.K., and Siddiqui, R.A. (2010). High ACAT1 expression in estrogen receptor negative basal-like breast cancer cells is associated with LDL-induced proliferation. Breast Cancer Res. Treat. *122*, 661–670.
51. Chen, M., and Huang, J. (2019). The expanded role of fatty acid metabolism in cancer: new aspects and targets. Precis. Clin. Med. *2*, 183–191.
52. Kamphorst, J.J., Cross, J.R., Fan, J., de Stanchina, E., Mathew, R., White, E.P., Thompson, C.B., and Rabinowitz, J.D. (2013). Hypoxic and Ras-transformed cells support growth by scavenging unsaturated fatty acids from lysophospholipids. Proc. Natl. Acad. Sci. USA *110*, 8882–8887.
53. Bensaad, K., Favaro, E., Lewis, C.A., Peck, B., Lord, S., Collins, J.M., Pinnick, K.E., Wigfield, S., Buffa, F.M., Li, J.L., et al. (2014). Fatty acid uptake and lipid storage induced by HIF-1α contribute to cell growth and survival after hypoxia-reoxygenation. Cell Rep. *9*, 349–365.
54. Damiano, F., De Benedetto, G.E., Longo, S., Giannotti, L., Fico, D., Siculella, L., and Giudetti, A.M. (2020). Decanoic Acid and Not Octanoic Acid Stimulates Fatty Acid Synthesis in U87MG Glioblastoma Cells: A Metabolomics Study. Front. Neurosci. *14*, 783.
55. Li, J.N., Gorospe, M., Chrest, F.J., Kumaravel, T.S., Evans, M.K., Han, W.F., and Pizer, E.S. (2001). Pharmacological inhibition of fatty acid synthase activity produces both cytostatic and cytotoxic effects modulated by p53. Cancer Res. *61*, 1493–1499.
56. Di Virgilio, F., Giuliani, A.L., Vultaggio-Poma, V., Falzoni, S., and Sarti, A.C. (2018). Non-nucleotide Agonists Triggering P2X7 Receptor Activation and Pore Formation. Front. Pharmacol. *9*, 39.
57. Ralevic, V., and Burnstock, G. (1998). Receptors for purines and pyrimidines. Pharmacol. Rev. *50*, 413–492.
58. Sorrentino, C., and Morello, S. (2017). Role of adenosine in tumor progression: focus on A_{2B} receptor as potential therapeutic target. J. Cancer Metastasis Treat. *3*, 127–138.
59. .http://www.cambridgesoft.com.
60. MOPAC2012, J.J.P.S. (2012). Stewart Computational Chemistry, Colorado Springs. HTTP://OpenMOPAC.net.
61. Pedretti, A., Villa, L., and Vistoli, G. (2004). VEGA–an open platform to develop chemo-bio-informatics applications, using plug-in architecture and script programming. J. Comput. Aided Mol. Des. *18*, 167–173.
62. Pedretti, A., Villa, L., and Vistoli, G. (2003). Atom-type description language: a universal language to recognize atom types implemented in the VEGA program. Theor. Chem. Acc. *109*, 229–232.
63. Yap, C.W. (2011). PaDEL-descriptor: An open source software to calculate molecular descriptors and fingerprints. J. Comput. Chem. *32*, 1466–1474.
64. Gramatica, P., Chirico, N., Papa, E., Cassani, S., and Kovarich, S. (2013). QSARINS: A new software for the development, analysis, and validation of QSAR MLR models. J. Comput. Chem. *34*, 2121–2132.
65. Gramatica, P., Cassani, S., and Chirico, N. (2014). QSARINS-chem: Insubria datasets and new QSAR/QSPR models for environmental pollutants in QSARINS. J. Comput. Chem. *35*, 1036–1044.
66. Mohamed, S.K., Mague, J.T., Akkurt, M., Abdu-Allah, H.H.M., and Albayati, M.R. (2015). Crystal structure of methyl 2-hy-droxy-5-[(4-oxo-4,5-di-hydro-1,3-thia-zol-2-yl) amino]benzoate. Acta Crystallogr. E Crystallogr. Commun. *71*, o282–o283.
67. El-Awady, R.A., Saleh, E.M., Ezz, M., and Elsayed, A.M. (2011). Interaction of celecoxib with different anti-cancer drugs is antagonistic in breast but not in other cancer cells. Toxicol. Appl. Pharmacol. *255*, 271–286.
68. Ning, Z., Cox, A.J., and Mullikin, J.C. (2001). SSAHA: a fast search method for large DNA databases. Genome Res. *11*, 1725–1729.
69. Li, H. (2012). Exploring single-sample SNP and INDEL calling with whole-genome de novo assembly. Bioinformatics *28*, 1838–1844.
70. Smith, T.F., and Waterman, M.S. (1981). Identification of common molecular subsequences. J. Mol. Biol. *147*, 195–197.
71. Lozon, L., Saleh, E., Menon, V., Ramadan, W.S., Amin, A., and El-Awady, R. (2022). Effect of safranal on the response of cancer cells to topoisomerase I inhibitors: Does sequence matter? Front. Pharmacol. *13*, 938471.
72. Ramadan, W.S., Vazhappilly, C.G., Saleh, E.M., Menon, V., AlAzawi, A.M., El-Serafi, A.T., Mansour, W., and El-Awady, R. (2018). Interplay between Epigenetics, Expression of Estrogen Receptor- alpha, HER2/ERBB2 and Sensitivity of Triple Negative Breast Cancer Cells to Hormonal Therapy. Cancers *11*, 13.
73. El-Awady, R.A., Semreen, M.H., Saber-Ayad, M.M., Cyprian, F., Menon, V., and Al-Tel, T.H. (2016). Modulation of DNA damage response and induction of apoptosis mediates synergism between doxorubicin and a new imidazopyridine derivative in breast and lung cancer cells. DNA Repair *37*, 1–11.
74. Trott, O., and Olson, A.J. (2010). AutoDock Vina: improving the speed and accuracy of docking with a new scoring function, efficient optimization, and multithreading. J. Comput. Chem. *31*, 455–461.
75. Semreen, M.H., Alniss, H.Y., Grgic, S.R., El-Awady, R.A., Almehdi, A.H., Mousa, M.K., and Hamoudi, R.A. (2019). Comparative metabolomics of MCF-7 breast cancer cells using different extraction solvents assessed by mass spectroscopy. Sci. Rep. *9*, 13126.
76. Wishart, D.S., Feunang, Y.D., Marcu, A., Guo, A.C., Liang, K., Vázquez-Fresno, R., Sajed, T., Johnson, D., Li, C., Karu, N., et al. (2018). HMDB 4.0: the human metabolome database for 2018. Nucleic Acids Res. *46*. D608-d617.
77. Alexandrov, L.B., Nik-Zainal, S., Wedge, D.C., Campbell, P.J., and Stratton, M.R. (2013). Deciphering signatures of mutational processes operative in human cancer. Cell Rep. *3*, 246–259.
78. Dieterle, F., Ross, A., Schlotterbeck, G., and Senn, H. (2006). Probabilistic quotient normalization as robust method to account for dilution of complex biological mixtures. Application in 1H NMR metabonomics. Anal. Chem. *78*, 4281–4290.
79. Benjamini, Y., Drai, D., Elmer, G., Kafkafi, N., and Golani, I. (2001). Controlling the false discovery rate in behavior genetics research. Behav. Brain Res. *125*, 279–284.
80. Storey, J.D. (2002). A direct approach to false discovery rates. J. Roy. Stat. Soc. B *64*, 479–498.

STAR★METHODS

KEY RESOURCES TABLE

REAGENT or RESOURCE	SOURCE	IDENTIFIER
Antibodies		
Anti- γH2AX Ser139	Cell signaling Technology	Cat # 9718, RRID:AB_2118009
Anti- H2AX	Cell signaling Technology	Cat # 2595, RRID:AB_10694556
Anti- p21	Cell signaling Technology	Cat # 2947, RRID:AB_823586
Anti- CDC2	Cell signaling Technology	Cat # 9116, RRID:AB_2074795
Anti-CDC25c	Cell signaling Technology	Cat # 4688, RRID:AB_560956
Anti- cyclin B1	Cell signaling Technology	Cat # 12231, RRID:AB_2783553
Anti- c-Myc	Cell signaling Technology	Cat # 9402, RRID:AB_2151827
Anti- Bid	Cell signaling Technology	Cat # 2002, RRID:AB_10692485
Anti- ATM	Cell signaling Technology	Cat # 2873, RRID:AB_2062659
Anti- *p*-ATM Ser1981	Cell signaling Technology	Cat # 5883, RRID:AB_10835213
Anti- ATR	Cell signaling Technology	Cat # 2790, RRID:AB_2227860
Anti- *p*-ATR	Cell signaling Technology	Cat # 2853, RRID:AB_2290281
Anti- Chk1	Cell signaling Technology	Cat # 2360, RRID:AB_2080320
Anti- *p*-Chk1 Ser348	Cell signaling Technology	Cat # 2348, RRID:AB_331212
Anti- Chk2	Cell signaling Technology	Cat # 6334, RRID:AB_11178526
Anti- *p*-Chk2 Thr68	Cell signaling Technology	Cat # 2661, RRID:AB_331479
Anti- caspase 9	Cell signaling Technology	Cat # 9508, RRID:AB_2068620
Anti- caspase 8	Cell signaling Technology	Cat # 9746, RRID:AB_2275120
Anti- p-Rb (Ser807/811)	Cell signaling Technology	Cat # 8516, RRID:AB_11178658
Anti- p53	Cell signaling Technology	Cat # 2524, RRID:AB_331743
Anti-cyclin A	Santa Cruz Biotechnology	Cat# sc-751, RRID:AB_631329
Anti- cyclin E	Santa Cruz Biotechnology	Cat# sc-247, RRID:AB_627357
Anti- cyclin D1	Santa Cruz Biotechnology	Cat # sc-753, RRID:AB_2070433
Anti- CDK2	Cell signaling Technology	Cat # 2546, RRID:AB_2276129
Anti- Rb	Santa Cruz Biotechnology	Cat # sc-50, RRID:AB_632339
Anti- p-Rb (Ser249)	Santa Cruz Biotechnology	Cat # sc-16671, RRID:AB_655229
Anti-β-actin	Sigma-Aldrich	Cat # A5441, RRID:AB_476744
Anti-Mouse IgG, HRP-linked	Cell signaling Technology	Cat # 7076, RRID:AB_330924
Anti-Rabbit IgG, HRP-linked	Cell signaling Technology	Cat # 7074, RRID:AB_2099233
Chemicals, peptides, and recombinant proteins		
DMSO	Sigma-Aldrich	Cat # 8418
Doxorubicin	Sigma-Aldrich	Cat #D1515
Protease/phosphatase inhibitors cocktail	Sigma-Aldrich	Cat # MSSAFE
Enhanced Chemiluminescence reagent	Biorad	Cat # 1705061
SYBR gold	Invitrogen	Cat #S11494
Critical commercial assays		
RNA extraction kit	Norgen Biotek	Cat # 17200
Comet assay kit	Trevigen	Cat # 4250-050-K
SuperScript VILO cDNA Synthesis kit	Invitrogen	Cat # 11754050

(*Continued on next page*)

Continued

REAGENT or RESOURCE	SOURCE	IDENTIFIER
Ion Library TaqMan™ Quantitation Kit	Applied Biosystems	Cat # 4468802
GoTaq qPCR master mix	Promega	Cat # A6001
FITC Annexin V Apoptosis Detection Kit	Becton Dickenson	Cat # 556547
Experimental models: Cell lines		
MCF7	University Medical Center Hamburg - Eppendorf	N/A
MDA-MB-231	University Medical Center Hamburg - Eppendorf	N/A
A549	University Medical Center Hamburg - Eppendorf	N/A
HCT116	University Medical Center Hamburg - Eppendorf	N/A
HepG2	University Medical Center Hamburg - Eppendorf	N/A
U87	University Medical Center Hamburg - Eppendorf	N/A
U373	University Medical Center Hamburg - Eppendorf	N/A
HeLa	University Medical Center Hamburg - Eppendorf	N/A
F180	University Medical Center Hamburg - Eppendorf	N/A
HME1	ATCC	Cat # CRL-4010
HCT116 CDK4 KO	University of Sharjah	N/A
Software and algorithms		
GraphPad Prism6	GraphPad	https://www.graphpad.com/scientificsoftware/prism/
ImageJ	ImageJ	https://imagej.nih.gov/ij/
Image Lab	Biorad	https://www.bio-rad.com/en-ae/product/image-lab-software?ID=KRE6P5E8Z
Rotor-gene Q	Qiagen	https://www.qiagen.com/kr/resources/resourcedetail?id=8435805b-2c5d-4fa9-948c-a43de75a7ee1&lang=en
Flow Jo	Tree Star	https://www.flowjo.com/
Ion Torrent Software Suite	Thermo Fisher Scientific	https://www.thermofisher.com/ae/en/home/life-science/sequencing/next-generation-sequencing/ion-torrent-next-generation-sequencing-workflow/ion-torrent-next-generation-sequencing-data-analysis-workflow/ion-torrent-suite-software.html
MSD Enhanced Chemstation	Shimadzu	https://www.shimadzu.com/an/products/gas-chromatograph-mass-spectrometry/gc-ms-software/index.html

RESOURCE AVAILABILITY

Lead contact

Further information and requests for resources and reagents should be directed to the lead contact, Raafat El-Awady (relawady@sharjah.ac.ae).

Materials availability

This study did not generate new unique reagents.

Data and code availability

- Data: All data reported in this paper will be shared by the lead contact upon request.
- Code: This paper does not report original code.
- Additional information: Any additional information required to reanalyse the data reported in this paper is available from the lead contact upon request

EXPERIMENTAL MODEL AND STUDY PARTICIPANT DETAILS

Cell lines and culture conditions

Eight different cancer cell lines were acquired from the Radiobiology and Experimental Radio Oncology lab, University Medical Center, Hamburg University, Hamburg, Germany. MCF7, MDA-MB-231 (breast cancer), and A549 (lung cancer) cells were maintained in RPMI medium while HCT116 (colon cancer), HepG2 (liver cancer), U87, U373 (glioblastoma), and HeLa (cervical cancer) were maintained in DMEM supplemented with 10% FBS and 1% penicillin/streptomycin (Sigma Aldrich, Missouri, USA). Normal human fibroblast (F180) cells were maintained in DMEM supplemented with 15% FBS. Normal human mammary epithelial cells (HME1) were maintained in DMEM/F-12 medium supplemented with 10% FBS. All incubations were done at 37°C in a humidified atmosphere of 5% CO2. All cell lines were authenticated by short tandem repeat (STR) profiling and were tested frequently for mycoplasma. The CDK4 knockout cells (provided by Dr. Samrein Ahmed, University of Sharjah, United Arab Emirates) were generated by CRISPR-CAS9 technology and were maintained in DMEM supplemented with 10% FBS.

METHOD DETAILS

Design of new 5-ASA-thiazolinone derivatives

The strategy in this discovery is the synthesis of pre-determined highly potent candidates calculated via *in silico* detection. Based on our previous effort,[12,13,26,27] we carried out a QSAR study to explore main structural features of our 5-Aminosalicylate-4-thiazolinone derivatives responsible for the proliferation inhibition pattern seen against MCF7 cancer cells. A database of a total 45 compounds with their corresponding percent inhibition data was established covering our previously reported compounds as well as the compounds presented herein. A multiple linear regression equation of eight parameters was used. This equation represents the best-developed model capable of describing the inhibitory pattern against MCF7 cancer cell line as illustrated below:

$$Log\ (\%inhibition) = -11.1958 - 0.0004 \times ATSC6v + 0.6379 \times AATSC6s + 45.2642 \times BCUTc_{1h} - 0.1102 \times maxHBint8 - 0.1040 \times WTPT_5 - 0.1676 \times RDF105m + 0.1258 \times RDF95e - 0.0328 \times RDF145i$$

$n = 44$, F-Statistic = 59.45, $R^2 = 0.931$, $Q^2_{LOO} = 0.893$, $Q^2_{LMO} = 0.837$, $R^2_{Y\text{-}scr} = 0.185$, $s = 0.129$.

Where in this equation, *ATSC6v* is centered Broto-Moreau autocorrelation of lag 6 weighted by van der Waals volumes; *AATSC6s* is average centered Broto-Moreau autocorrelation of lag 6 weighted by I-state; *BCUTc-1h* is *n*low highest partial charge weighted BCUTS; *maxHBint8* is maximum E-state descriptors of strength for potential hydrogen bonds of path length 8; *WTPT-5* is sum of path lengths starting from nitrogens; *RDF105m* is radial distribution function-105 weighted by relative mass; *RDF95e* is radial distribution function-095 weighted by relative Sanderson electronegativities; *RDF145i* is radial distribution function-145 weighted by relative first ionization.

The model was found to fit the experimental percent inhibition of MCF7 (Figure 2) with considerable level of significance as indicated by its high Fischer's value (F), squared correlation coefficients (R^2) and the minor standard errors of estimate. The presented model is specific to our compound's chemo-type, thus their internal predictive power was judged based on leave-one-out (*LOO*) and leave-many-out (*LMO*) procedures. The probability of chance correlation was examined by Y-scrambling procedure, in which, lower ($R^2_{Y\text{-}Scr}$) value indicates lesser probability of chance correlation. The internal validation parameters achieved by the model demonstrates its reliability and robustness in predicting new derivatives within our series and could be utilized for future development.

The most influential variables that are in direct relation with the bioactivities were identified by the model as; *AATSC6s, BCUTc-1h* and *RDF95e*. Those variables have favorable contribution to the overall activity as indicated by their positive coefficients and are basically demonstrating the importance of structural electronic properties (ionization states, partial charges and electronegativities). These conclusions are in agreement with our previous findings regarding the influence of electron-donating and electron-withdrawing substituents.[27]

Quantitative structure-activity relationship (QSAR)

The compounds were drawn using ChemDraw Ultra 8.0 software[59] and for each compound, the lowest energy conformation was generated using MOPAC2012[60] within VEGA-ZZ software.[61,62] Austin Model-1 (AM1) semi-empirical force-field was employed for this purpose. PaDEL-software[63] was used for molecular descriptors calculations. The software calculates a large set of 1D-3D molecular descriptors (*ca.* 1875) of different classes including constitutional, topological, information indices, eigenvalue-based indices, radial distribution function (RDF), 2D/3D autocorrelation. The calculated descriptors were served as independent variables during QSAR model development. The logarithmic values of experimentally observed percent inhibition against MCF7 cancer cell line were served as the dependent variable. The QSAR models were developed and validated employing the QSARINS software.[64,65] Model development process was initiated by reducing co-linearity (corr. > 0.98) and excluding the descriptor showing higher pairwise correlation with others. All subsets procedure was adapted for the first two variables. Next, the optimal combinations of variables (>2) relevant to the dependent variable under study were selected using a genetic algorithm (GA). During the GA variables selection phase, the population size, maximum number of generations, and mutation rate were set to 800, 2000, and 0.2 respectively. Multiple linear regression method was used for the final model building. The final model's robustness was validated employing internal predictive measures based on Q^2_{LOO} (leave one-out), Q^2_{LMO} (leave many-out), and $R^2_{Y\text{-}scr}$ (Y-scrambling).

Calculations suggested candidates **HH32** and **HH33** providing up to 100% growth inhibition. The candidates were then synthesized and subjected to pharmacological investigation.

Synthesis of acetylated 5-ASA-thiazolinone derivatives HH32 and HH33

The synthesis of the target compounds is described in Scheme 1. Different approaches were tried for acetylation. The one described herein was found to be the most convenient. Starting compound **1** was synthesized as reported,[27] then acetylated with acetic anhydride in presence of catalytic H_2SO_4 to give compound **2**. Heterocyclization of **2** with ammonium thiocyanate gave **HH31**.

Knovenagel condensation of **HH31** with 4-methylbenzaldehyde or 4-dimethylaminobenzaldehyde provided the target compounds **HH32 and HH33**, respectively. All compounds were fully characterized by spectral data (spectral copies of synthesized compounds are provided as supporting information). From ^{1}H NMR spectra, a characteristic doubling of the signals is observed in the cyclized products (**HH31**-**HH33**) which indicates the presence of syn/anti arrangement of rotamers (Figure 3).

The presence of two rotamers (conformers) is already known for 2-arylamino-2-thiazolin-4-ones and was confirmed by ^{1}H NMR signal integration and X-ray crystal structure.[13,66] The ratio of the two rotamers in solution was approximately (1:1) based on ^{1}H NMR signal integration.

All reagents and solvents were obtained from commercial suppliers and used without further purification. Melting points are uncorrected and were determined on an electrothermal melting point apparatus (Stuart Scientific, model SM.P.3, England, UK). Precoated silica gel plates (kieselgel 0.25 mm, 60G F254, Merck, Germany) were used for TLC monitoring of reactions. UV light was used for detection. NMR spectra were recorded on Bruker AMX400 MHz instruments (Data S1). Chemical shifts were reported in ppm and are referenced to the chemical shift of residual solvent.

Methyl 2-acetoxy-5-(chloroacetamido) benzoate (2)

To compound **1** (2.00 g, 8.20 mmol) in Ac_2O (5 mL), was added one drop of conc H_2SO_4. The reaction mixture was stirred at room temperature for 2 h. To the reaction mixture, ice water was added, rapidly filtered and dried to give pure white product. (2.13 g, 92.5% yield); ^{1}H NMR (400 MHz, $CDCl_3$) δ = 8.43 (br. s., 1H, NH), 8.03 (d, 1H, *J* = 4 Hz, Ar-H), 8.03 (d, 1H, *J* = 4 Hz, Ar-H), 7.83 (d, 1H, *J* = 4 Hz, Ar-H), 7.06 (d, 1H, *J* = 4 Hz, Ar-H), 4.16 (s, 2H, CH_2), 3.86 (s, 3H, OCH_3); 2.35 (s, 3H, CH_3); ^{13}C NMR (100 MHz, $CDCl_3$) δ = 170.07 (C=O of acetate), 164.3 (C=O of ester), 164.2 (C=O of amide), 147.2 (aromatic C), 134.7 (aromatic C), 125.4 (aromatic C), 124.4 (aromatic C), 123.4 (aromatic C), 123.0 (aromatic C), 52.4 (OCH3), 42.8 (CH_2Cl), 20.9 (CH_3 of acetate).

Synthesis of methyl 2-acetoxy-5-[(4,5-dihydro-4-oxo-1,3-thiazol-2-yl)-amino]benzoate (HH31)

A solution of **2** (12.57 g, 44 mmol) and ammonium thiocyanate (7.00 g, 91.2 mmol) in 150 mL ethanol was refluxed for 2 h, cooled to room temperature and allowed to stand overnight at this temperature. The mixture was concentrated and filtered. The collected solid was washed with water, recrystallized from ethanol/water and dried to give (9.72 g, 72%); m.p. = 185–187°C. ^{1}H NMR (400 MHz, DMSO-*d6*) δ = 11.90, 11.40 (2*s, 1H; NH), 8.27, 7.99 (2*d, *J* = 4 Hz, 1H, ArH-6), 7.48 (br. s., 1/2H, ArH-4), 7.30–7.22 (m, 1.5H, ArH-4, ArH-3), 4.05, 4.02 (2*s, 2H, CH_2), 3.83, 3.81 (2*s, 3H; OCH_3), 2.28 (s, 3H, CH_3); ^{13}C NMR (100 MHz, DMSO-*d6*) δ = 188.6 (C=O), 179.1 (C=O), 169.8 (C=O), 164.6 (C=O), 146.8 (aromatic C), 146.6 (aromatic C), 137.1 (aromatic C), 127.6 (aromatic C), 126.1 (aromatic C), 125.5 (aromatic C), 125.2 (aromatic C), 123.9 (aromatic C), 123.7 (aromatic C), 122.9 (C=N), 52.9 (CH_2), 52.8 (OCH_3), 21.1 (CH_3).

General procedure for synthesis of methyl 2-acetoxy-5-[(5-benzylidene -4-oxo-4,5-dihydro-1,3-thiazol-2-yl)-amino]benzoate (HH32, HH33)

To a well-stirred solution of compound **HH31** (0.43 g, 1.4 mmol) in acetic acid (10 mL) buffered with sodium acetate (0.18 g, 2.2 mmol), the appropriate benzaldehyde (1.6 mmol) was added. The solution was refluxed for 24 h till the completion of the reaction as monitored by TLC, cooled to room temperature, and then poured into ice-cold water. The precipitate was filtered, and the resulting crude product was purified by recrystallization from dioxane.

Methyl 2-acetoxy-5-[(5-(4-methylbenzylidene)-4-(*H*)-oxo-1,3-thiazol-2-yl)-amino]benzoate (**HH32**) (0.43 g, 75% yield); m.p. = 218–220°C; R_f = 0.4 (hexane/ethyl acetate; 2/1); ^{1}H NMR (400 MHz, DMSO-*d6*) δ = 12.49, 11.80 (2*s, 1H; NH), 8.36, 8.08 (2*d, *J* = 4 Hz, 1H, ArH-6), 7.73, 7.69 (2*d, *J* = 4 Hz, 1H, ArH-4), 7.54–7.51 (m, 2H, CH = C, ArH-3), 7.42–7.28 (m, 4H, 4-CH_3Ph), 3.91, 3.83 (2*s, 3H; OCH_3), 2.37, 2.31 (2*s, 6H; CH_3); ^{13}C NMR (100 MHz, DMSO-*d6*) δ = 179.7 (C=O), 170.6 (C=O), 168.8 (C=O), 168.7 (C=O), 163.5 (C=O), 146,1 (aromaic C), 145.9 (aromaic C), 139.5 (aromaic C), 135.7 (aromaic C), 130.5 (aromaic C), 130.4 (aromaic C), 129.8 (aromaic C), 129.4 (aromaic C), 129.3 (aromaic C), 129.2 (aromaic C), 129.0 (aromaic C), 126.3 (aromaic C), 125.3 (aromaic C), 125.2 (aromaic C), 124.6 (aromaic C), 124.3 (aromaic C), 123.2 (aromaic C), 122.9 (aromaic C), 122.7 (aromaic C), 122.1 (aromaic C), 120.9 (C=N), 51.9 (OCH_3), 51.8 (OCH_3), 20.4 (CH_3), 20.1 (CH_3).

*Methyl 2-acetoxy-5-[(5-(4-dimethylaminobenzylidene)-4-(*H*)-oxo-1,3-thiazol-2-yl)- amino]benzoate (HH33)*

(0.43 g, 70% yield); m.p. = 234–235°C; R_f = 0.2 (hexane/ethyl acetate; 2/1); ^{1}H NMR (400 MHz, DMSO-*d6*) δ = 10.41 (br. S, 1H, NH), 8.30, 8.05 (2*d, *J* = 4 Hz, 1H, ArH-6), 7.65–7.25 (m, 5H; ArH-4, CH = C, ArH-2′,6′ 4-$(NMe_2)C_6H_4$), 7.02–7.10 (m, 1H; ArH-3), 6.80, 6.70 (2*d, *J* = 8.0 Hz, 2H; ArH-3′,5′ 4-$(NMe_2)C_6H_4$), 3.92, 3.88 (2*s, 3H; OCH_3), 3.00, 2.95 (2*s, 6H, $N(CH_3)_2$, 2.30 (s, 3H, Me). ^{13}C NMR (100 MHz, DMSO-*d6*) δ = 180.2 C=O), 169.8 C=O), 169.1 C=O), 164.6 C=O), 151.5 (aromaic C), 132.0 (aromaic C), 131.7 (aromaic C), 125.6 (aromaic C), 124.0 (aromaic C), 121.8 (aromaic C) 114.0 (aromaic C), 112.5 (C=N), 53.1 (OCH_3), 53.0 (OCH_3), 21.1 (NCH_3).

HH32 and HH33 compounds preparation

Stock solutions of **HH32** and **HH33** compounds were prepared in 100% Dimethyl sulfoxide (DMSO) (Sigma Aldrich, Missouri, USA) and the working solutions of compounds didn't exceed 0.1% DMSO.

Cytotoxicity assay

The cytotoxic effects of **HH32** and **HH33** compounds were evaluated at various concentrations ranging from 0.0001 to 100 μM by sulphrhodamine-B (SRB) assay as described previously.[67] The anti-proliferative activity was expressed as growth inhibitory concentration (IC_{50}) values, which were calculated by the sigmoidal dose-response curve fitting method using Graph pad prism 6 software (GraphPad Software, San Diego, CA, USA).

Transcriptomic analysis

MCF7 and A549 cells were harvested after treatment with IC_{50} doses of **HH33** compound for 24 h (0.81μM for MCF7 and 2.93μM for A549). RNA extraction was carried out followed by cDNA synthesis using SuperScript VILO cDNA Synthesis kit (Invitrogen, Waltham, MA, USA) and amplification using Ion AmpliSeq gene expression core panel primers. The prepared library was purified using Agencourt AMPure XP beads (Beckman Coulter, California, USA) and quantified using Ion Library TaqMan Quantitation Kit (Applied Biosystems, Waltham, MA, USA). The libraries were further diluted to 100p.m. and pooled equally with four individual samples per pool. The pooled libraries were amplified using emulsion PCR on Ion OneTouch 2 instrument (OT-II) and the enrichment was performed on Ion OneTouch ES following the manufacturer's instruction. Thus, prepared template libraries were then sequenced with Ion S5 XL Semiconductor sequencer using the Ion 540 Chip.

RNA-seq data were analyzed using Ion Torrent Software Suite version 5.4 and the alignment was carried out using modifications of the Torrent Mapping Alignment Program (TMAP) optimizing it for aligning the raw sequencing reads against reference sequence derived from hg19 (GRCh37) assembly. The specificity and sensitivity was maintained by implementing a two-stage mapping approach by employing BWA-short, BWA-long, SSAHA,[68] Super-maximal Exact Matching[69] and Smith Waterman algorithm[70] for optimal mapping. Raw read counts of the targeted genes were performed using Samtools (Samtools view –c –F 4 –L bed_file bam_file) and the number of expressed transcripts was confirmed after Fragments Per Kilobase Million (FPKM) normalisation. Differentially expressed gene (DEG) analysis was performed using a script written in R programming language (version 3.6.3) with function calls to DESeq2 package from Bioconductor library sets. Raw read counts from RNASeq were normalized using quantile normalization. All counts ranked "0" were excluded. Differentially expressed genes between the two set of cell lines [**HH33**-treated (n = 3), and untreated (n = 3)] were assessed using 2 tailed t-test. Differentially expressed genes with p value of <0.05, adjusted p value <0.8 and 5-fold difference were included for pathway analysis using Metascape.

Western blot

The protein expression analysis was done after treatment with 0.5 or 1μM of **HH32** and **HH33** compounds for 24 h by Western blot.[26] Cell lysates were prepared using lysis buffer containing 20% SDS, glycerol, 1M Tris (pH 6.8) and supplemented with protease and phosphatase inhibitors (Sigma Aldrich, Missouri, USA). The proteins were separated by SDS-PAGE and transblotted into nitrocellulose membrane (Biorad, Hercules, CA, USA). Membrane were incubated overnight at 4°C with the following primary antibodies: γH2AX, H2Ax, p21, CDC2, CDC25c, cyclin B, c-Myc, Bid, ATM, *p*-ATM, ATR, *p*-ATR, Chk1, *p*-Chk1, Chk2, *p*-Chk2, caspase 9, caspase 8, pRb (Ser807/811) (Cell Signaling Technology, Massachusetts, USA), p53, cyclin A, cyclin E, cyclin D1, CDK2, Rb, pRb (Ser249) (Santa Cruz Biotech, Texas, USA) and β-actin (Sigma Aldrich, Missouri, USA). Membranes were then incubated with respective mouse/rabbit secondary antibody (Cell Signaling Technology, Massachusetts, USA) for 1 h at room temperature and detected by enhanced chemiluminescence (ECL) (Biorad, Hercules, CA, USA) method using Chemi Doc imaging system (Biorad, Hercules, CA, USA). The protein bands were quantified using Image lab software (Biorad, Hercules, CA, USA).

Neutral comet assay

MCF7, HCT-116 and A549 cells were treated with 0.5 or 1μM of **HH32** or **HH33** compounds for 24 h and control cells were treated with vehicle (DMSO). A group of cells was treated with doxorubicin as a reference drug using the same treatment conditions. Comet assay was performed in neutral condition to detect DNA double-strand breaks using comet assay kit (Trevigen Inc., Maryland, USA) according to the manufacturer's instructions.[71] The tail moment, which reflect the amount of DNA damage in each nucleus, was calculated in at least 50 cells using OpenComet software.

Cell cycle analysis

The effect of the **HH32** and **HH33** compounds on the distribution of cell cycle at different time points (2, 4, 8, 24, 48, and 72 h) was analyzed using flow cytometry.[72] Briefly, the cells were harvested and fixed in 70% ethanol for 24 h at −20°C. The fixed cells were treated with RNAase (100 μg/ml) (Sigma Aldrich, Missouri, USA) and stained with propidium iodide (50 μg/ml) (Sigma Aldrich, Missouri, USA). The data were acquired using BD Accuri C6 flow cytometer (Becton Dickenson, San Jose, CA, USA) and analysis was done using Flow Jo software (Tree Star, Inc, Ashland, OR, USA).

Apoptosis analysis

The cells were collected at 12, 24 and 48 h after treatment with 0.5 or 1μM of **HH32** and **HH33** compounds. The detection of early and late apoptotic cell death was done using FITC Annexin V Apoptosis Detection Kit (Becton Dickenson, California, USA) according to the manufacturer's protocol.[73] The data were analyzed by BD Accuri C6 flow cytometer (Becton Dickenson, New Jersey, USA).

Molecular docking studies

Molecular docking studies were performed employing the program Autodock Vina.[74] X-ray crystal structures for the proteins under study, namely; Cdc25C, CDK1/Cyclin-B1, CDK2/Cyclin-A and retinoblastoma tumor suppressor (Rb) protein were downloaded from Protein DataBank (http://www.rcsb.org/pdb/) under the entry codes of; 3OP3, 4Y72, 6GUE and 1O9K, respectively. Complexed inhibitors and water molecules were extracted from their initial X-ray structures. Later, Autodock Tools (MGL Tools 1.5.6rc2) were utilized for adding polar hydrogens and generating Gasteiger charges. The compounds under study were treated employing the same mentioned procedure. Additionally, grid boxes were established to cover the active site on each macromolecule, with a spacing of 1.0 Å between the grid points, centered toward their respective coordinates. The exhaustiveness and the number of poses were set to 14 and 10, respectively.

Metabolic analysis

The release of different metabolites following **HH32** and **HH33** treatment on MCF7 cells was detected using Gas Chromatography-Mass Spectrometry (GC-MS) (Shimadzu, Kyoto, Japan) as was described previously.[75] GC-MS analysis was performed using a QP2010 gas chromatography-mass spectrometer (GC-2010 coupled with a GC-MS QP-2010 Ultra) equipped with an auto-sampler (AOC-20i+s) from Shimadzu (Tokyo, Japan), using Rtx-5ms column (30 m length × 0.25 mm inner diameter × 0.25 μm film thickness; Restek, Bellefonte, PA, USA). Helium (99.9% purity) was used as the carrier gas with the column flow rate of 1 mL/min. Data collection and analysis were performed using MSD Enhanced Chemstation software (Shimadzu, Kyoto, Japan). GC total ion chromatograms (TIC) and fragmentation patterns of the compound were identified using the NIST/EPA/NIH Mass Spectral Library (NIST 14).

Preprocessing and data analysis were performed using an in-house R script. Only compounds registered in Human Metabolome Database (HMDB 4.0)[76] were considered for further analysis. Compounds with more than 70% of missing values were considered unreliable and therefore excluded. Probabilistic Quotient Normalization[77] was used to normalize data due to dilution effects in the extraction procedure. Missing metabolite measurements were imputed using the k-nearest neighbor algorithm[78] with $k = 3$. Student's t test was used to identify significantly ($p < 0.05$) altered metabolites for each drug. To account for multiple testing, a false discovery rate (FDR) of <15% was applied to reduce the identification of false positives. FDRs were calculated using the q conversion algorithm[79,80] in multiple comparisons. Principal component analysis (PCA) was used to visualize the metabolomic data (Figure S9). Data were mean-centered and scaled to unit variance before PCA.

QUANTIFICATION AND STATISTICAL ANALYSIS

The data were described as mean ± standard error of the mean (SEM) of at least three independent experiments. Unpaired Student's t test was used to compare **HH32**/**HH33**- treated samples to DMSO-treated samples. p value <0.05 was considered statistically significant. All statistical calculations were done by GraphPad Prism 6 (GraphPad Software, San Diego, CA, USA).